AMERICAN UNIVERSITY OF BEIRUT

DEGREES OF FREEDOM AND IMPAIRMENTS IN MASSIVE MIMO SYSTEMS

by
WISSAM OUSSAMA ABDESSAMAD

A thesis
submitted in partial fulfillment of the requirements
for the degree of Master of Engineering
to the Department of Electrical and Computer Engineering
of the Faculty of Engineering and Architecture
at the American University of Beirut

Beirut, Lebanon
September 2016

AMERICAN UNIVERSITY OF BEIRUT

DEGREES OF FREEDOM AND IMPAIRMENTS IN MASSIVE MIMO SYSTEMS

by

WISSAM OUSSAMA ABDESSAMAD

Approved by:

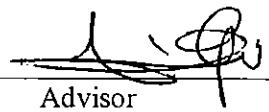

Prof. Youssef Nasser, Senior Lecturer
Electrical and Computer Engineering — Advisor

Prof. Hassan Ali Artail, Professor
Electrical and Computer Engineering — Member of Committee

Prof. Ali Chehab, Professor
Electrical and Computer Engineering — Member of Committee

Date of thesis defense: September 9, 2016

AMERICAN UNIVERSITY OF BEIRUT

THESIS, DISSERTATION, PROJECT RELEASE FORM

Student Name: _____
Last First Middle

○ Master's Thesis ○ Master's Project ○ Doctoral Dissertation

☐ I authorize the American University of Beirut to: (a) reproduce hard or electronic copies of my thesis, dissertation, or project; (b) include such copies in the archives and digital repositories of the University; and (c) make freely available such copies to third parties for research or educational purposes.

☐ I authorize the American University of Beirut, **three years after the date of submitting my thesis, dissertation, or project,** to: (a) reproduce hard or electronic copies of it; (b) include such copies in the archives and digital repositories of the University; and (c) make freely available such copies to third parties for research or educational purposes.

_____

Signature Date

ACKNOWLEDGMENTS

I would like to thank first my advisor Prof. Youssef Nasser who has been my main guide throughout this thesis. I am really grateful for all the help and advice you have given me.

I would like to thank my parents and sister who have encouraged me to do my Master's Degree at AUB. Your support was really a key factor for my success.

AN ABSTRACT OF THE THESIS OF

Wissam Oussama Abdessamad for Master of Engineering
Major: Electrical and Computer Engineering

Title: Degrees of Freedom and Impairments in Massive MIMO Systems

Massive multiple-input multiple-output (MIMO) systems is an emerging technology that is paving its way into wireless communication systems. Massive MIMO consists of tens or hundreds of antennas, which will result in huge increase in capacity, reliability and performance. However, massive MIMO is facing complexity issues in terms of channel estimation, RF impairments and RF design due to the large number of antennas.

On the other hand, sparse code multiple access (SCMA) is a multi-dimensional system with codebook based on non-orthogonal coding technique offering high bitrate. It is presented as one of the potential candidates for LTE-A systems and beyond. In SCMA, the procedure of bit to QAM symbol mapping and spreading are combined and incoming bits are directly mapped to multi-dimensional codewords of SCMA codebook sets.

In this thesis, we explore degrees of freedom and constraints offered in the combination of SCMA-MIMO systems in terms of capacity and RF impairments. The interest of MIMO-SCMA resides in the need of lower number of antennas while preserving the system capacity thanks to the overload in SCMA. Using some properties from Random Matrix and free probability theories, we derive analytical approximations of the Signal to Interference and Noise Ratio (SINR) and capacity expressions in the presence of RF impairments (mainly carrier frequency offset and phase noise) of the combined systems. The latter are independent of the code design but depend on the code length and the overload factor. We show that there is exists a tradeoff between SCMA and MIMO in terms of performance and complexity. All derivations are validated by extensive simulation results.

CONTENTS

ILLUSTRATIONS

Figure Page

TABLES

CHAPTER 1

INTRODUCTION

This chapter presents an overview of Multiple Input Multiple Output (MIMO) systems highlighting the need of such systems in future genrations of communication systsms. In addition, it explains the importance of adding Sparse Code Multiple Access Technique (SCMA) to MIMO. Finally, this chapter presents an outline for the thesis.

1.1. MIMO Overview

Next generation wireless communication systems demand highly reliable, spectrally efficient and high data rate schemes. Today, many systems respond to these demands by adopting advanced techn0ologies such as Multiple Input Multiple Output (MIMO), Device-to-Device (D2D), small cells, etc. This includes various wireless standards such as 3GPP-LTE, IEEE 802.16m, IEEE 802. 11n [1]-[2].

Recently, Massive MIMO [3]-[4] and Sparse Code Multiple Access (SCMA) schemes were proposed as other potential candidate for 5G networks. Massive MIMO systems preserve not only all the advantages of conventional MIMO systems but go beyond on a much larger scale [5]; these systems consist of tens and sometimes hundreds of antennas at the base station serving a large number of users over the same time/frequency resources. Furthermore, they can achieve very high gains in both spectral efficiency and energy efficiency compared to technologies in 4G systems. However, this is obtained at the detriment of an increased complexity of the hardware, an increased energy consumption and a complexity of the signal processing at both ends[6][7].

Although massive MIMO makes numerous traditional research problems irrelevant, it reveals entirely new problems that needs a crucial attention. For instance, the challenge of making several low-cost low-precision components work efficiently together, the necessity for effective acquisition scheme for channel state information, the exploitation of extra degrees of freedom provided by a surplus of service antennas, resource allocation for newly-joined terminals, decreasing internal power consumption to attain total energy efficiency reductions, and finding new deployment scenarios [8]-[9].

1.2. SCMA Overview

On the other hand, the SCMA promises significant enhancements to communication systems in terms of throughput [10][11]-[12]. SCMA is a non-orthogonal codebook-based multiple-access technique with near optimal spectral efficiency. SCMA is seen as a particular spreading scheme where binary data is mapped to multi-dimensional complex codewords, designed in a non-orthogonal way so that different spread data are superimposed before transmission. The main interest of the SCMA scheme resides in the possibility of resources overloading by mapping different data layers (users) to the same resources without Channel State Information (CSI) between paired users. However, this is obtained at the cost of additional complexity at the receiver due to the non-orthogonal nature of the super-imposed data [12].

1.3. Motivation and Objectives

In this research, a combination of MIMO and SCMA techniques in one transmission scheme is proposed. Particularly, the performance of layered spatial

multiplexing MIMO schemes with SCMA is analyzed, and uncoded and coded Bit Error Rate (BER) results are provided.

Moreover, Phase noise is a topic of theoretical and practical interest in electronic circuits. Though improvement has been made in the representation of its description, there are still significant gaps in its effects especially on multi carrier systems. Due to the implementation of large number of subcarriers, the MIMO-SCMA system become highly sensitive to Carrier Phase Noise (CPN). In our work, the effect of CPN on the MIMO-SCMA system is modeled and using some properties of random matrix and free probability theory, a simplified expression of the Signal to interference and noise ratio (SINR) is obtained after equalization.

1.4. Thesis Structure

The remainder of this thesis is organized as follows: Chapter 2 is a litterature review on MIMO systems, massive MIMO systems and SCMA systems. Chapter 3 presents the first part of this thesis: *A MIMO-SCMA system and its performance in terms of coded and uncoded bit error rate*. Chapter 4 presents the second part of this thesis: *RF impairments in MIMO-SCMA-OFDM system*. It presents the of our proposed system where the effect of carrier frequency offset (CFO) and carrier phase noise (CPN) can be modeled, and by using some properties of random matrix and free probability theory the analytical SINR is obtained. Chapter 5 presents the conclusion of this thesis and the future work.

CHAPTER 2

LITERATURE REVIEW

This chapter provides first a literature review of MIMO systems, massive MIMO systems, and SCMA systems highlighting there advantages and disadvantages.

2.1. MIMO Systems

The wireless system designers are confronted by many challenges to satisfy the demand of the wireless communication for enhanced quality service (QoS) , greater data rates, less dropped calls , much higher network capacity taking into consideration the limited availability of radio frequency spectrum and transmission difficulties triggered by numerous factors like fading and multipath. These needs necessitates new techniques that increase operational reliability and spectral efficiency. Multi-Input-Multi-Output (MIMO) technology promises a cost effective technique to offer these capabilities.

MIMO utilizes multiple antennas at both the transmitter and receiver to increase the communication performance in many aspects. MIMO technology has attracted attention in wireless communications, because it provides important growths in data throughput and link range without any extra bandwidth or transmit power. It attains this by greater spectral efficiency and link reliability or diversity (reduced fading). Because of these properties, MIMO is a current theme of international wireless research.

The growing demand for capacity in wireless systems has inspired significant research intended at realizing improved throughput on a certain bandwidth. One key new discovery demonstrates that in a multipath environment, the usage of space-time coding

with multiple antennas on both ends of the communication link can rise the capacity of the wireless channel. MIMO algorithms sends data over multiple paths, thus improving the amount of information the system carries and the data is received by multiple antennas and recombined properly by other algorithms to recover the data at the receiver. MIMO is a fundamental technique for carrying data. It works at the physical layer, below the protocols used to carry the data, so its channels can work with virtually any wireless transmission protocol. Therefore, MIMO ultimately will become the standard for carrying almost all wireless traffic. MIMO the only economical way to increase bandwidth, range and will become a core technology in wireless systems. Assessing the performance of these algorithms requires detailed understanding of multiple-input multiple-output (MIMO) channels as well as models that capture their complex spatial behavior [13].

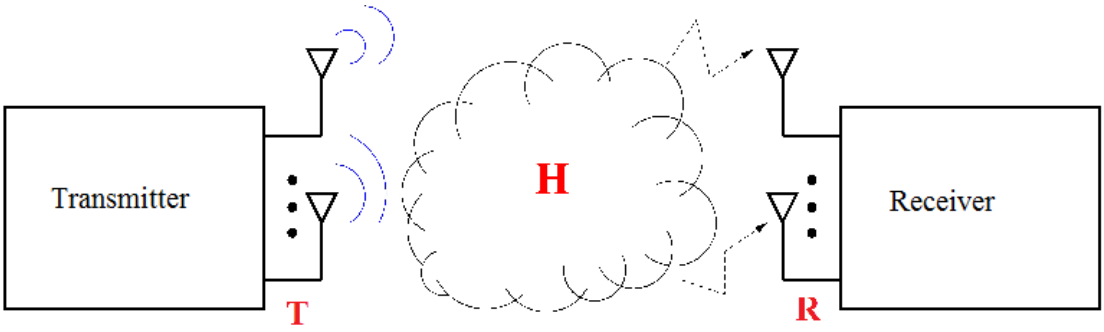

Fig. 1: MIMO System Model

2.2. Massive MIMO Systems

Multiple-antenna (MIMO) technology is becoming complete for wireless communications and has been integrated into wireless broadband standards like Wi-Fi and LTE. Essentially, the more antennas the transmitter/receiver is equipped with, the more the possible signal paths and the more improved the performance in terms of link

reliability and data rate. The price to pay is increased complexity of the hardware (the number of RF amplifier frontends) and the complexity and energy consumption of the signal processing at both ends.

Massive MIMO (also known as Large-Scale Antenna Systems, Very Large MIMO, Hyper MIMO, Full-Dimension MIMO and ARGOS) makes a clean break with current practice through the use of a very large number of service antennas (e.g., hundreds or thousands) that are functioned fully adaptively and coherently. Additional antennas help by focusing the transmission and reception of signal energy into ever-smaller regions of space. This brings enormous improvements in throughput and energy efficiency, mainly when joined with simultaneous scheduling of a large number of user terminals (e.g., tens or hundreds). Massive MIMO was initially planned for time division duplex (TDD) operation, but can actually be applied also in frequency division duplex (FDD) operation. Other benefits of massive MIMO include the extensive use of inexpensive low-power components, reduced latency, simplification of the media access control (MAC) layer, and robustness to interference and intentional jamming. The anticipated throughput depends on the propagation environment providing asymptotically orthogonal channels to the terminals, and experiments have so far not disclosed any limitations in this regard. While massive MIMO renders many traditional research problems irrelevant, it uncovers entirely new problems that urgently need attention. For example, the challenge of making many low-cost low-precision components work effectively together, the need for efficient acquisition scheme for channel state information, resource allocation for newly-joined terminals, the exploitation of extra degrees of freedom provided by an excess of service antennas, reducing internal power consumption to achieve total energy efficiency reductions, and finding new deployment scenarios [14].

Practically realizing massive MIMO systems is not easy. The complexity of numerous algorithms for MIMO increases exponentially with the increase in number of antennas. Even linear increase in complexity is unaffordable when the number of antennas is very large. The restraining factors of massive MIMO include, but are not restricted to, pilot contamination, channel reciprocity, which is required for time division duplex (TDD) mode, orthogonality of channel response, and radio propagation. Four major research trends to boost massive MIMO performance are channel estimation, resource allocation, downlink precoding and data detection for massive MIMO.

Channel estimation is essential for coherent detection at the receiver. However, it becomes impractical when the number of antennas is great, which is the reason why most of the researches about massive MIMO systems generally assume perfect channel state information (CSI) knowledge at the transmitters [15]-[16]. Furthermore, many studies are conducted on energy efficient resource allocation for Massive MIMO systems for both downlink and uplink scenarios, with analysis on the achievable data rates [17], and optimal number of antennas to be selected to maximize the signal to noise ratio (SNR) at the receiver [18]. Precoding strategies are signal processing techniques used to reduce the interference and also a dynamic research topic for massive MIMO. Additionally, when it comes to detection, the major concern with moving to massive MIMO is the high detection complexities. Therefore, the work on the detection level is targeted to find detection algorithms that are practically implementable and that can attain good performance as well [19].

2.2.1. Advantages of Massive MIMO Systems

Massive MIMO systems have several advantages, among whih are: a high improvement of spectral and energy efficiency, the system can be built at low cost and low power consumption (which reduces the total transmit power), which allows a significant reducation of the latency in the air interface; increase the robustness of the system. The linear precoding techniques are optimal, the thermal noise, the fading and the intra-cells interferences are practically eliminated, allowing an important capacity gain.

2.2.1.1. Improvement of Spectral and Energy efficiency

In the Massive MIMO system, using the precoding/beamforming techniques and operating in the green" regime (considerably reducing the transmit power without reducing the spectral efficiency), the interference of the multi-users and the effects of the material imperfections tend to vanish. Therefore, the energy efficiency is N times improved (N is the number of antennas at the base station). Additionally, because tens of users are served simultaneously with the same time/frequency resources, the total spectral efficiency can be ten times bigger than ten classic MIMO systems. In a way, Massive MIMO is based on the Law of Large Numbers that is applied on a very large number of antennas, lead the noise, the fading and the imperfections to cancel when the signals coming from a very large number of antennas are combined together in the radio interface. The drastic improvement in the energy efficiency allows the Massive MIMO to operate with a total transmit power two times less than the current technologies. And then, the base state consuming low energy can be fed with solar energy in places lacking electricity. Moreover, the fact to have less transmitted energy reduce the electromagnetic

interferences; because the gain in energy have a reciprocity. The preceding advantages can also be applied to the terminals. That permits the users to have less battery constraints while benefiting from high data rate. This is also important to reduce the expositions to the electromagnetic rays. [20] It was also proved that the linear precoding/beamforming techniques are optimal when the transmit power is considerably reduced.

2.2.1.2. Latency Reduction on the Radio Interface

Generally, the latency is the time delay to the users caused by fading situations (a user having a bad channel is not served)). Because the massive MIMO systems are based on the precoding/beamforming techniques and the law of large numbers to almost cancel the fading, the latency time is significantly reduced.

2.2.1.3. Robustness

The same arguments (precoding/beamforming and the low of large numbers) are valid when a strange signal is sent (considered as noise); then in using the beamforming with a number of antennas N (very large), the emitted signal is canceled. Additionally, the same properties that make the massive MIMO systems robust to the fading are also the cause of keeping the same performance of the capacity when one or more antennas are not in the functional state.

2.2.2. Drawbacks and Open Issues

2.2.2.1. Pilot Contamination

Ideally, every terminal in a massive MIMO system is assigned to pilot sequence in the uplink in a way that the pilot sequences are orthogonal. On the other hand, there is

a maximal number of orthogonal pilot sequences that can be produced (based on the coherence time and delay spread [21]). Because the number of users is not limited by a fixed particular number, pilot sequences should be reused in neighboring cells; that could cause the phenomenon called Pilot Contamination. More specifically, when the antenna correlates its received pilot signal of an UE with the same pilot signal used by another UE allocated in a neighboring cell, this antenna gets an estimated channel that is the linear combination of the channels of the users using the same pilot sequence. The more N is large, the more the pilot contamination can be an annoying factor.

The pilot contamination can be easily faced by the use of certain techniques. Based on the correlation, the pilot sequences can be attributed to users based on second order statistics of the channel (when they are known), this permits the reduction of this contamination, the blind estimation based on EVD [22]-[23], the precoding based on the pilot contamination [24], the decrease of the time of pilots [25].

2.2.2.2. PAPR Effect

When using low cost components at the RF chains of Massive MIMO systems, the amplifiers become less good quality. When we use OFDM in these systems, we will have a high Peak to Average Power Ratio (PAPR) due to the non-linearity of the amplifiers. We can limit this problem by using OFDM because the objective in the use of OFDM is to get less inter-symbol interference (ISI) for a simpler equalization; or with massive MIMO systems having orthogonal channels we have less ISI and thus we can use single carrier transmissions and therefore limiting the PAPR effect.

2.3. Sparse Code Multiple Access Systems

In order to improve spectral efficiency, MIMO systems utilize multiple antennas at both the transmitter and the receiver. Nevertheless, in order to allow simultaneous transmissions to multiple users over the same time and frequency resource elements, MIMO forms an extended version of space-division multiple access called multi-user MIMO (MU-MIMO) [3]-[4]-[26]-[27]. MU-MIMO is a new multiple access technique aiming at sharing power and time-frequency resources among users [28]. Even though the simplicity of detection at the user nodes offers promising throughput gain, MU-MIMO is highly limited by technical constraints such as channel aging, overhead ratio of the channel state information (CSI) of users to a serving access point (AP). This could consequently lead to a potential performance limitation and transmission gain of the MU-MIMO system.

Open-loop user multiplexing is another approach to bypass practical limitations of MU-MIMO. Non-orthogonal code domain multiple-access such as SCMA, is an open-loop system to couple multiple users over shared time-frequency resources [11]-[12]. SCMA (mainly MU-SCMA) is recommended to increase a network throughput. With a very small requirement for channel knowledge in terms of channel quality indicator (CQI), APs pairs users together while the transmit downlink power is accurately shared among multiplexed layers. When compared to MU-MIMO, SCMA system is obviously more robust against channel variations. Furthermore, the problem of CSI feedback is entirely eliminated for this open-loop multiple-access scheme. The main problem however of SCMA is the non-orthogonal multiple access scheme. Indeed, the layers are not fully separated, therefore a non-linear receiver is required to detect the intended layer of every user. Thus, additional complexity of detection is the cost of the non-orthogonal

multiple-access especially when a system is overloaded with a huge number of multiplexed layers. Sparsity of SCMA codewords allows the usage of the low complexity message passing algorithm (MPA) [29] detector with ML-like performance even when the system is overloaded with a large number of layers.

To improve spectral efficiency of linear sparse sequences through multidimensional shaping gain of codebooks while still providing other benefits in terms of overloading and moderate complexity of detection, the SCMA digital modulation (such as QAM) mapper is merged with the sparse spreading operation to directly map the incoming bits into codewords [30]. The robustness of the link quality and interference management are very important issues to deal with in lightly loaded networks. The resource exploitation drops when the traffic demand is low. Within the long-term evolution (LTE) [31] context, as a case of an OFDMA system, that is comparable to muting of some resource blocks (RB) across the bandwidth of an AP. Spreading over OFDMA tones can possibly advance the quality of link-adaptation process due to the interference averaging [10]. This leads the interference to be white, which has the benefit of better and more robust link-adaptation. Moreover, layer multiplexing adds an additional degree of freedom to the link-adaptation proficiency of an SCMA system. Number of layers beside the coding rates, codebook sizes, and power level of multiplexed layers are the parameters controlling the rate and quality of a link [32].

2.3.1. SCMA Transmission System

The block diagram of the SCMA transmission system is shown in Fig. 2 below:

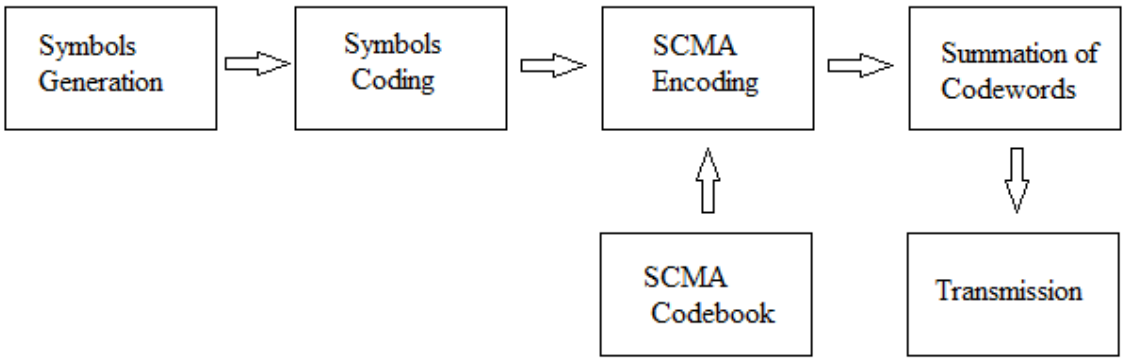

Fig. 2: SCMA Transmission System

In SCMA scheme, the generated bits are firstly fed to a channel encoding, such as Turbo coding. The signal is then fed to the SCMA encoder using a codebook. The SCMA encoder is a mapping from $\log_2(M)$ coded bits to a N_F -dimensional complex codeword chosen from a SCMA codebook with a size M constellation [11], and the elements of the selected N_F -dimensional complex codeword will be additionally mapped into N_F orthogonal dimensions for transmission. The N_F -dimensional complex codewords in a SCMA codebook are sparse vectors with W non-zero elements, where W should be relatively small with respect to N_F in order to maintain an acceptable level of sparsity. For example, if W=2, 2-dimensional constellation points can be mapped over N_F resources. The mapping graph of the codewords in SCMA codebook can be built by all possible combinations of the N_F -dimensional vectors with W non-zero entries. Therefore, the number of SCMA codebooks is $N_u = \binom{N_F}{W}$, and the resultant overloading factor (OF) will be $OF = \frac{N_u}{N_F}$.

The mapping graph of the codewords in SCMA codebook is symbolized as $\boldsymbol{F}_{W,N_F}$, and the j-th column of $\boldsymbol{F}_{W,N_F}$ $(1 \leq j \leq N_u)$is the vector defining the location of non-zero entries for the j-th codeword in the SCMA codebook. For instance, if W=2, N_F=4, $\boldsymbol{F}_{W,N_F}$can be given by a $N_F \times N_u$ matrix as

$$\boldsymbol{F}_{W,N_F} = \begin{bmatrix} 011010 \\ 101001 \\ 010101 \\ 100110 \end{bmatrix}. \quad (1)$$

The SCMA codebook is designed by multiplying the matrix mapping the W dimensions of a constellation point to a N_F-dimensional SCMA codeword with the constellations points according to a predefined factor graph representation. Hence, each symbol is mapped to a particular codeword in a particular codebook for each layer. At the end, the codewords from each layer are added together and transmitted.

2.3.2. SCMA Reception System

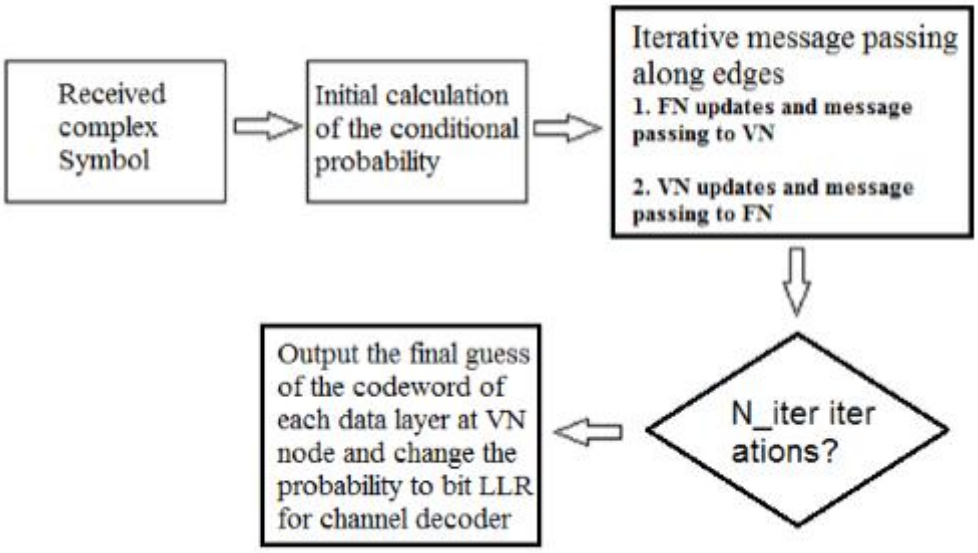

Fig. 3: SCMA Reception System

The SCMA receiver shown in Fig. 3. is divided into several steps.

Step 1: Receiving the signal $\boldsymbol{y}$

$$\boldsymbol{y} = diag(\boldsymbol{h}) \sum_{j=1}^{N_u} \boldsymbol{x}_j + \boldsymbol{e} \quad (2)$$

where $\boldsymbol{h}$ is the channel matrix of dimensions $1 \times N_F$, $\boldsymbol{x}_j$ is the transmitted complex symbol from user j of dimensions $N_F \times 1$, and $\boldsymbol{e}$ is the Additive White Gaussian Noise (AWGN) of dimensions $N_F \times 1$.

Step 2: Message Passing Algorithm

Message Passing Algorithm (MPA) is a classical receiver algorithm for SCMA. The process of MPA can be described by the factor graph as shown in Fig. 4 for $N_F = 4$ and $N_u = 6$.

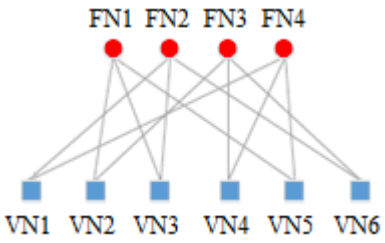

Fig. 4: Factor Graph Representation of MPA

- *Step 2.1: Initial calculation of the conditional probability for each resource block*

$$f_n = -\frac{1}{N_{0,n}} \left\| y_n - \left(\sum_{i=1}^{df} h_{n,i} \boldsymbol{C_{i,g}}(m_i) \right) \right\|^2 \quad (3)$$

$$with\ m_i = 1, \dots, M \text{ and } n = 1, \dots, N_F$$

f_n is the set of all possible residual signals given the known or estimated channel coefficient and the assumed transmitted codeword, f_n is of dimensions $1 \times M^{df}$, where df is the number of connected variable nodes (VN) to each function node (FN).

From the f_n function, the conditional probability for a given combination of codewords can be obtained, as follows:

$$p(y|x_1, x_2, \dots, x_{df}) = e^{f_n} \quad (4)$$

For each layer, $p(y|x_1, x_2, \dots, x_{df})$ is an array of size M^{df}. The a-priori probability for each codeword (for each layer) is

$$P(x_1) = P(x_2) = \cdots = P(x_{df}) = \frac{1}{M} \tag{5}$$

- *<u>Step 2.2:</u> Iterative message passing along edges*

  1) FN update for each FN node g, which then passes the extrinsic information to its neighboring VN nodes VNq (g to VN1, information from VN2 and VN3 are extrinsic) [33].

$$\boldsymbol{I}_{g\to VNq}(m_q) = \sum_{m_{i\neq q}=1}^{\boldsymbol{M}} \dots \sum_{m_{j\neq q}=1}^{\boldsymbol{M}} f_n \prod_{\substack{i=1 \\ i\neq q}}^{df} \boldsymbol{I}_{VNi\to g}(m_i) \tag{6}$$

  2) VN update for each VN node, which then passes the extrinsic information to its neighboring FN nodes g_q(VN to g_1, information from $g_2$is extrinsic) [33].

$$\boldsymbol{I}_{VN\to g_q}(m) = \frac{1}{M}\boldsymbol{I}_{g_{i\neq q}\to VN(m)} \tag{7}$$

- *<u>Step 2.3:</u> LLR output at variable node after N_iter iteration*

$$\boldsymbol{Q_{VNq}}(m) = \frac{1}{M}\prod_{\substack{i=1 \\ i\neq q}}^{\boldsymbol{dv}} \boldsymbol{I}_{g_i\to VNq}(m) \tag{8}$$

where $Q_{VNq}(m)$ is the probability guess of codeword m at each layer, and dv is the number of connected FN to each VN.

$$\begin{aligned} LLR_x = \quad & \log\left(\frac{\sum_{m:b_{m,x=0}} Q_{VNq}(m)}{\sum_{m:b_{m,x=1}} Q_{VNq}(m)}\right) \\ & = \log\left(\sum_{m:b_{m,x=0}} Q_{VNq}(m)\right) - \log\left(\sum_{m:b_{m,x=1}} Q_{VNq}(m)\right) \end{aligned} \tag{9}$$

CHAPTER 3

MIMO-SCMA SYSTEM

This chapter presents the first part of the thesis: *A MIMO-SCMA system and its performance in terms of coded and uncoded bit error rate*. It explains the system model, the results of our implementation, the analysis of the obtained results and a conclusion of this first part.

3.1. MIMO-SCMA System Model

The MIMO-SCMA system is obtained by extending equation 2, where the number of transmitting antennas and the number of receiving antennas are increased to *T* and *R* respectively. Hence, the received signal at each antenna *r* could be written as:

$$\boldsymbol{Y}^{(r)} = \sum_{t=1}^{T} \boldsymbol{H}^{(r)(t)} \boldsymbol{X}^{(t)} + \boldsymbol{E}^{(r)} \tag{10}$$

$$\text{where } \boldsymbol{Y}^{(r)} = \begin{pmatrix} y_1^{(r)} \\ \vdots \\ y_{N_F}^{(r)} \end{pmatrix},\ 1 \le r \le R \tag{11}$$

$$\boldsymbol{H}^{(r)(t)} = \begin{pmatrix} h_1^{(r)(t)} & \cdots & 0 \\ \vdots & \ddots & \vdots \\ 0 & \cdots & h_{N_F}^{(r)(t)} \end{pmatrix}, \quad \begin{matrix} 1 \le r \le R \\ 1 \le t \le T \end{matrix} \tag{12}$$

$$\boldsymbol{X}^{(t)} = \begin{pmatrix} x_1^{(t)} \\ \vdots \\ x_{N_F}^{(t)} \end{pmatrix}, \quad 1 \le t \le T \tag{13}$$

$$\boldsymbol{E}^{(r)} = \begin{pmatrix} e_1^{(r)} \\ \vdots \\ e_{N_F}^{(r)} \end{pmatrix}, \quad 1 \le r \le R \tag{14}$$

H is the channel matrix of dimensions $N_F R \times N_F T$ and **E** is the additive white Gaussian noise of dimensions $N_F R \times 1$.

At the receiving side, different types of equalizations are firstly applied. In this paper, the conventional MIMO equalization schemes are used.

Zero-Forcing Equalization (ZF):

$$\begin{cases} \boldsymbol{Z} = \boldsymbol{H}^{-1}\boldsymbol{Y} & , for\ T = R \quad (15) \\ \boldsymbol{Z} = (\boldsymbol{H}^{H}\boldsymbol{H})^{-1}\boldsymbol{H}^{H}\boldsymbol{Y} & , for\ T \neq R \quad (16) \end{cases}$$

$$\text{where } \boldsymbol{Z} = \begin{pmatrix} \boldsymbol{Z}^{(1)} \\ \vdots \\ \boldsymbol{Z}^{(T)} \end{pmatrix} \quad (17)$$

$$\boldsymbol{Z}^{(t)} = \begin{pmatrix} z_1^{(t)} \\ \vdots \\ z_K^{(t)} \end{pmatrix}, 1 \leq t \leq T \quad (18)$$

$$\boldsymbol{H} = \begin{pmatrix} \boldsymbol{H}^{(1)(1)} & \dots & \boldsymbol{H}^{(1)(T)} \\ \vdots & \ddots & \vdots \\ \boldsymbol{H}^{(R)(1)} & \dots & \boldsymbol{H}^{(R)(T)} \end{pmatrix} \quad (19)$$

- Minimum Mean Square Error Equalization (MMSE):

$$\widehat{\boldsymbol{X}} = \left(\boldsymbol{H}^{H}\boldsymbol{H} + \boldsymbol{N_0}\boldsymbol{I_{TN_F}}\right)^{-1}\boldsymbol{H}^{H}\boldsymbol{Y} \quad (20)$$

where $\boldsymbol{N_0}$ is the noise variance and $\boldsymbol{I_{TN_F}}$ is the identity matrix of size $T \times N_F$.

Once equalized, the signal is firstly fed to the SCMA decoder followed by a turbo decoder. An iterative process is then applied until it converges.

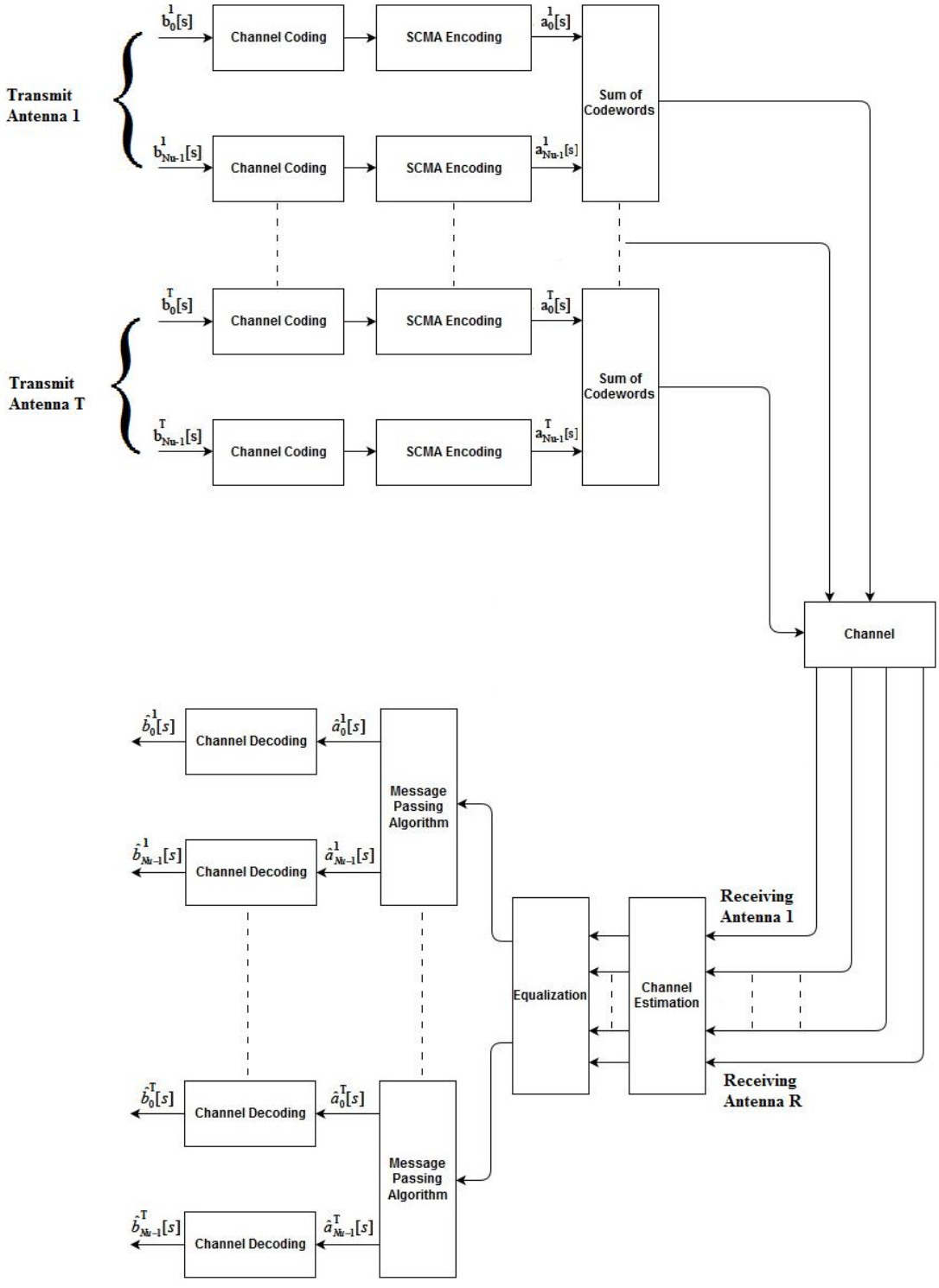

Fig. 5: MIMO-SCMA Block Diagram

3.2. Simulation Results

In this section, some simulation results of the MIMO-SCMA scheme are provided. The simulation parameters are given in TABLE 1.

Table 1: Simulation Parameters for MIMO-SCMA System

Simulation Parameter	Value
Constellation size (M)	BPSK, QPSK, 16-QAM
Number of resource blocks (N_F)	4
Number of Layers (N_u)	6
Overloading factor (N_u/N_F)	1.5
Dimensions of factor graph (F)	4x6
f_j : column of F	$diag(V_j V_j^T)$, $1 \leq j \leq N_u$

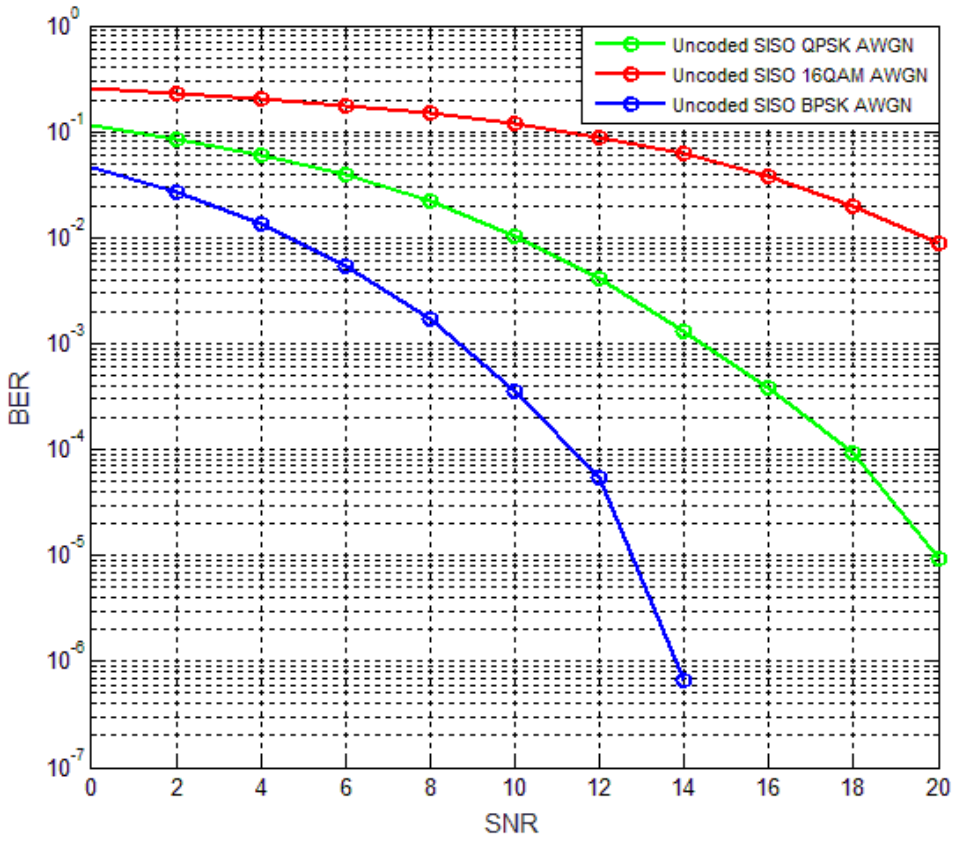

Fig. 6: Uncoded SISO-SCMA, BPSK, QPSK, and 16-QAM modulations, ZF Equalization, AWGN channel

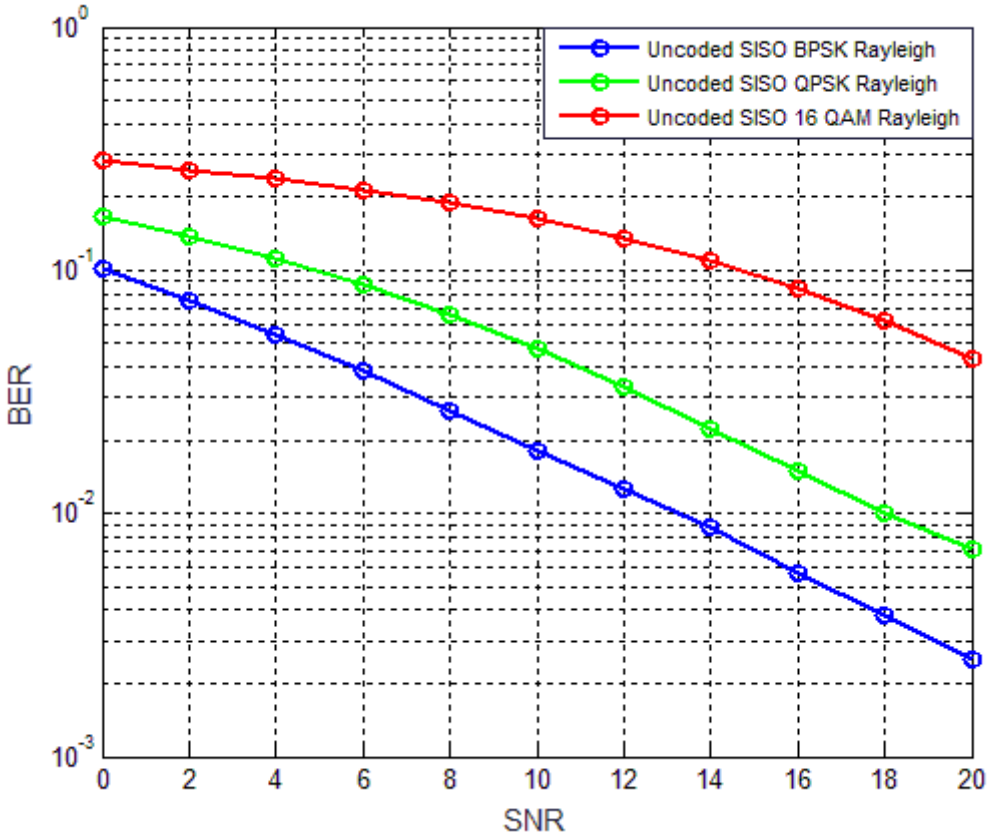

Fig. 7: Uncoded SISO-SCMA, BPSK, QPSK, and 16-QAM modulations, ZF Equalization, Rayleigh channel

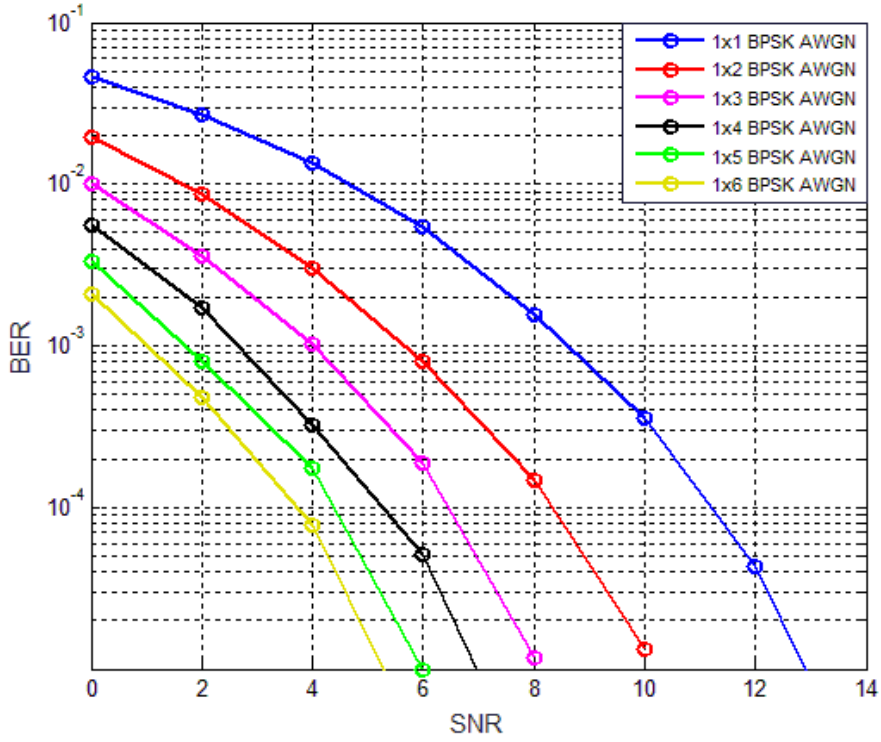

Fig. 8: Uncoded SIMO-SCMA, BPSK modulation, MMSE Equalization, AWGN channel

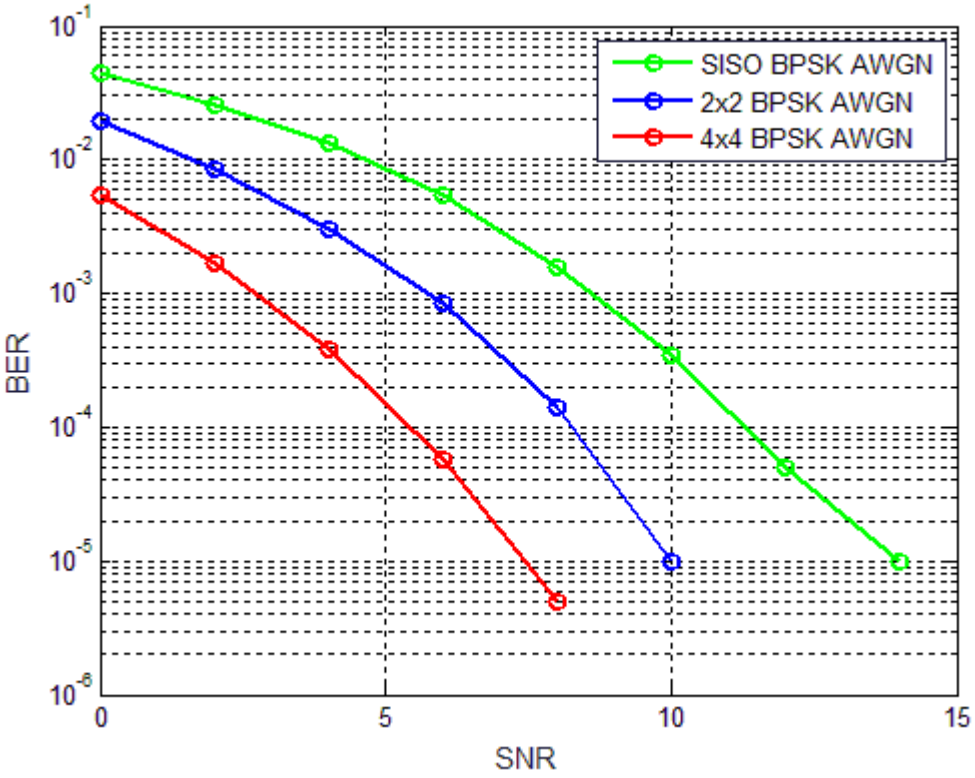

Fig. 9: Uncoded MIMO-SCMA, BPSK modulation, ML-detection, AWGN channel

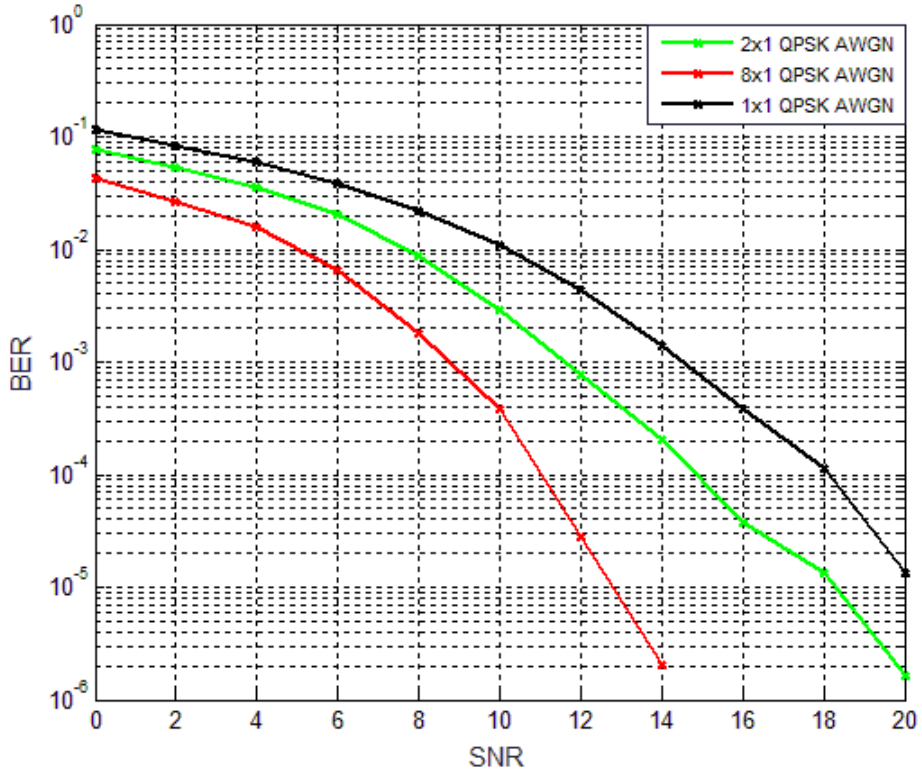

Fig. 10: Uncoded MISO-SCMA, QPSK modulation, ML-detection, AWGN channel

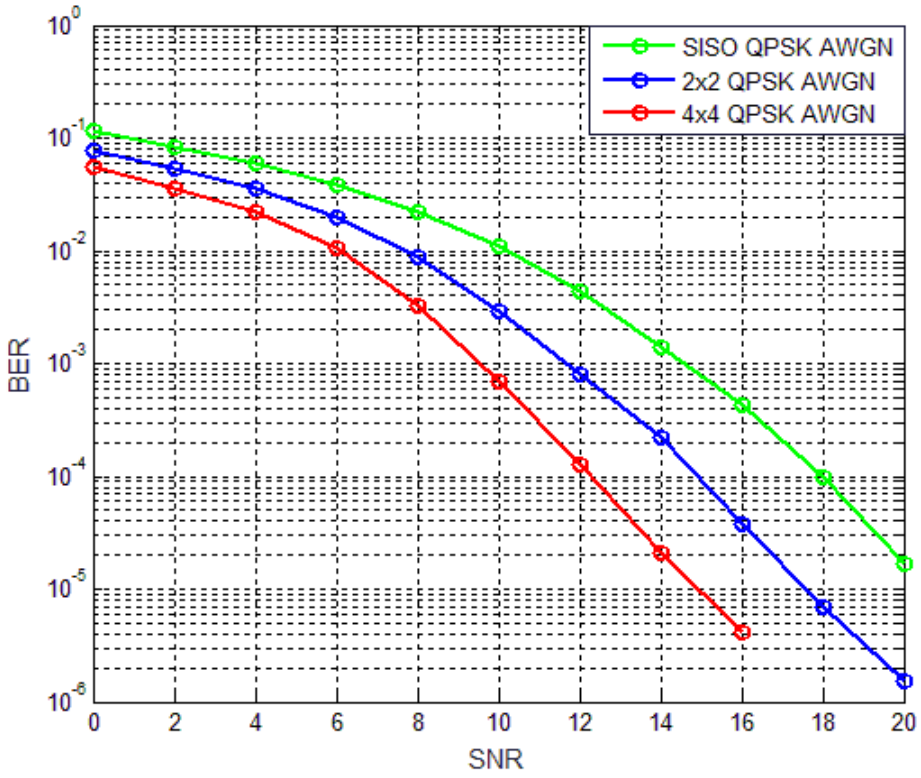

Fig. 11: Uncoded MIMO-SCMA, QPSK modulation, ML-detection, AWGN channel

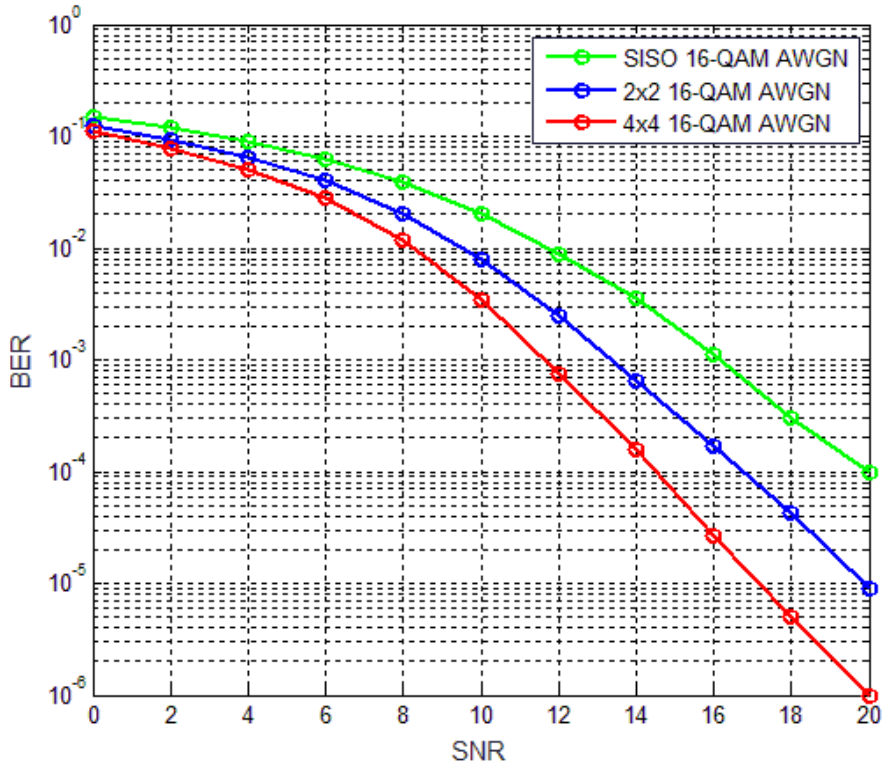

Fig. 12: Uncoded MIMO-SCMA, 16-QAM modulation, ML-detection, AWGN channel

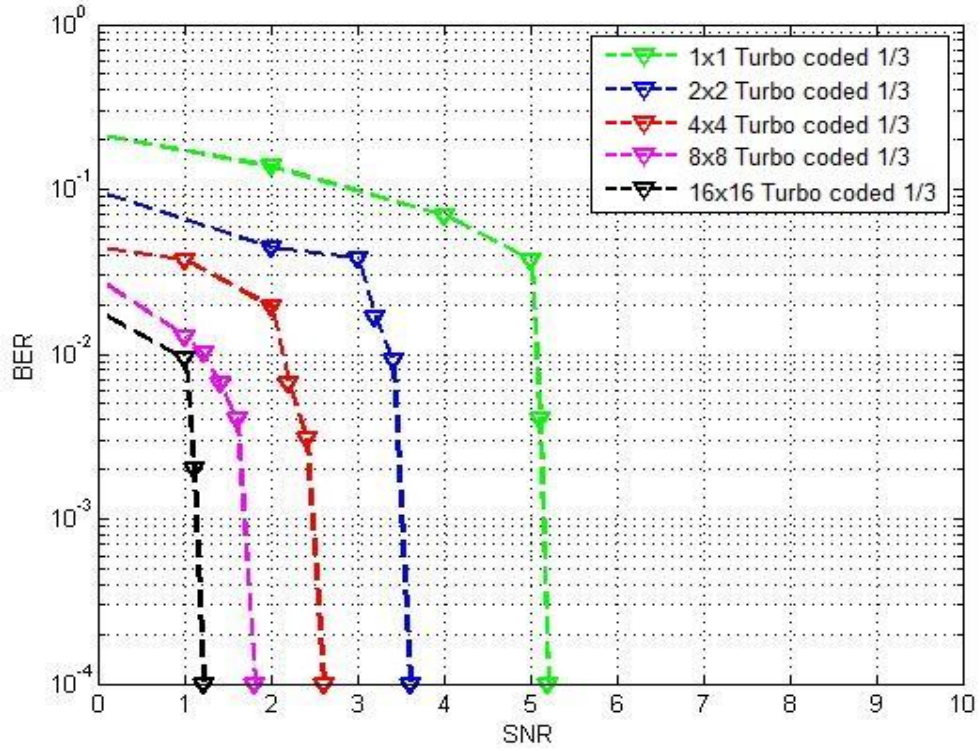

Fig. 13: Turbo coded MIMO-SCMA, rate=1/3, QPSK modulation, MMSE Equalization, AWGN channel

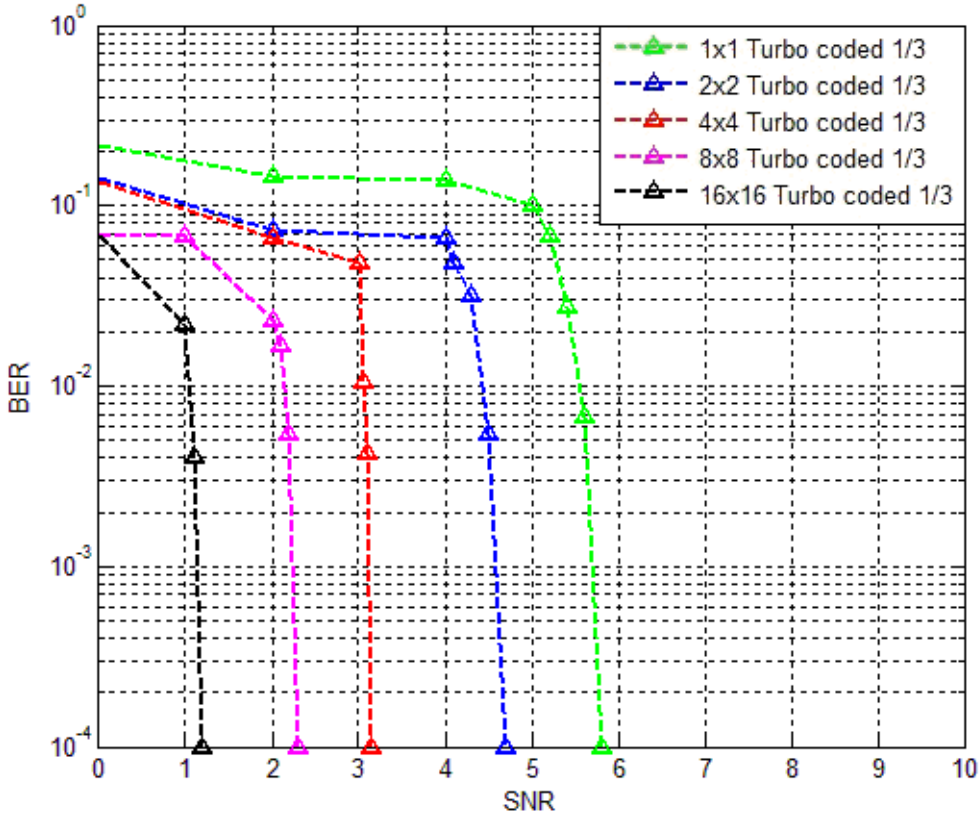

Fig. 14: Turbo coded MIMO-SCMA, rate=1/3, QPSK modulation, MMSE Equalization, Rayleigh channel

Figures 6 and 7 show the performance of SCMA system with BPSK, QPSK and 16-QAM modulation schemes in AWGN and Rayleigh channels respectively, these results demonstrated the accuracy of our SCMA simulations before we upgraded the system into MIMO-SCMA, these results matches the results in the literature in [46] and [47] respectively. In Figure 8, we started by increasing the number of receiving antennas in the SCMA system to have a SIMO-SCMA; we realize that for the same BER the SNR decrease by 3dB when the number of receiving antennas is doubled. In figures 9 to 14 we can see a better performance in terms of BER as we have a gain in power as we increase the number of antennas in the transmitter and/or the receiver in Rayleigh and AWGN channel in both uncoded and Turbo coded systems.

3.3. Results Analysis

If we compare between figures 11 and 12 for example, we can see that in QPSK has better performance than 16-QAM, so we can see that the performance of 4x4 16-QAM is same as 2x2 in QPSK, which is very accurate result due to the difference in the energy per bit between the two modulation schemes.

CHAPTER 4

RF IMPAIRMENTS IN MIMO-SCMA-OFDM SYSTEM

This chapter presents the second part of this thesis: *RF impairments in MIMO-SCMA-OFDM system*. It presents the of our proposed system where the effect of carrier frequency offset (CFO) and carrier phase noise (CPN) can be modeled, and by using some properties of random matrix and free probability theory the analytical SINR is obtained.

4.1. Carrier Offset

4.1.1. Carrier Frequency offset

Carrier frequency offset (CFO) is one of numerous impairments in baseband receiver scheme. When designing a baseband receiver, we should observe not only the degradation created by non-ideal channel and noise, we should consider as well RF and analog parts.

Carrier frequency offset usually happens when the local oscillator signal of down-conversion in the receiver is not synchronized with the carrier signal of the received signal. Such occurrence can be credited to two essential factors: frequency mismatch between the transmitter and the receiver oscillators; and the Doppler effect cause by the motion of the transmitter or the receiver.

Once this happens, the received signal will be shifted in the frequency domain. For an OFDM system, only if the receiver utilizes a local oscillation signal that is synchronous with the carrier of the received signal then the orthogonality among sub carriers will be preserved. Otherwise, the incompatibility in carrier frequency can cause inter-carrier

interference (ICI). On further notice, the oscillators in the transmitter and the receiver are never oscillating at the same frequency. Therefore, the CFO always occurs even with the absence of the Doppler effect.

In Continuous-Time domain:

$$\boldsymbol{y(t) = x(t)e^{-j(2\pi \Delta f t + \theta)} * h(t) + e(t)} \tag{21}$$

In Discrete-Time domain:

$$\boldsymbol{y[k] = (x[k] * h[k])e^{-j(2\pi k \Delta F T_s + \theta)} + e[k]} \tag{22}$$

In Frequency domain:

$$\begin{aligned} \boldsymbol{Y[p]} &= \boldsymbol{X[p]H[p]e^{j\pi((N-1)\Delta F T_s)} \times \frac{1}{N} \frac{sin(p-n-N\Delta F T_s)}{sin\left(\frac{p-n-N\Delta F T_s}{N}\right)}\Big|_{p=n}} \\ &+ \sum_{\substack{n=0 \\ n \neq p}}^{N-1} \boldsymbol{X[n]H[n]e^{-j\pi(p-n-N\Delta F T_s)\left(1-\frac{1}{N}\right)} \times \frac{1}{N} \frac{sin(p-n-N\Delta F T_s)}{sin\left(\frac{p-n-N\Delta F T_s}{N}\right)}\Big|_{p \neq n}} \\ &+ \boldsymbol{E[p]} \end{aligned} \tag{23}$$

4.1.2. Carrier Phase Noise Model

To achieve high spectrum efficiency, MIMO-SCMA systems will implement a great number of resource blocks and, consequently, will be highly sensitive to the carrier phase noise (CPN) [34]. The effect of the CPN could be similar of that caused by a constant carrier frequency offset (CFO) i.e. CPN presents a phase rotation on the received complex symbols and creates inter-carrier interference (ICI). Nevertheless, in contrary to the CFO, the CPN is a random process. Then, it should be studied alone in order to

evaluate its effects. In the literature, we find several works on the CFO and its effects on the multicarrier based systems [34][35]-[36].

In order to model the effect of CPN on the MIMO-SCMA system, OFDM will be inserted in the system to become a MIMO-SCMA-OFDM system as shown in Figure 15.

In a multi-carrier transmission scheme like MIMO-SCMA-OFDM, the CPN produces two effects: common phase error (CPE) and Inter Carrier Interference (ICI). The CPE modifies equivalently different carriers by initiating sub-carrier phase rotation while ICI introduces interference to any sub-carrier from all other sub-carriers. In the literature, the CPN effect was been presented in some papers for OFDM [34]-[37]-[38]-[39].

In this chapter, a new approach to present the degradation caused by the CPN on the performance of the MIMO-SCMA-OFDM systems is proposed. Our contribution is based on the work done in [40] which was done for a CPN in the OFDM-CDMA system. It is also based on previous works done for different synchronization errors [41]-[42]-[43].We consider that the CPN is with small angle approximation and also without small variation approximation.

Using some properties of random matrix (RM) and free probability (FP) theories, we develop a new analytical expression of the SINR in an asymptotic regime. This SINR formula depends on the complex amplitudes of the channel coefficients, the average transmitted power of the interfering users, the affected power of the reference user, the number of users and the number of subcarriers.

A frequency synthesizer utilize a voltage-controlled oscillator (VCO) to generate a certain range of frequencies from a one oscillator. Nevertheless, due to electronic impairments and circuits imperfections, the frequency synthesizer cannot operate with a

peak at the working radio frequency f_0, and frequency fluctuations will spread the oscillator power over neighboring sidebands. The term Carrier Phase Noise (CPN) is generally utilized to define short-term frequency fluctuations of the oscillator. The sidebands are usually decreasing for a certain frequency f_m selected reasonably far from the central carrier. The CPN is measured in dBc/Hz at a particular offset where dBc characterizes dB relative to the carrier. It can be described in time domain as a continuous Brownian motion process with a zero mean and a variance equal to $2Dt$ where D is the CPN line-width known as diffusion factor [44]. This phase noise has independent Gaussian increments, which can be described as a finite-power Wiener phase whose spectrum drops with the inverse of the frequency's square. In discrete time illustration, the CPN can be attained iteratively at each time sample k as:

$$\varepsilon\,[k+1] = \varepsilon[k] + \rho[k] \tag{24}$$

where $\varepsilon[k]$ is the sampled CPN and $\rho[k]$ is a Gaussian random variable with zero mean and variance equal to $2DT_s$ where T_s is the sampling period. The CPN PSD is written as:

$$S_\varepsilon(f) = \frac{2D}{D^2 + (2\pi f)^2} \tag{25}$$

The oscillator is included in a Phase Locked Loop (PLL) controlled by an ultra-stable oscillator operating at low frequency to decrease the sidebands. When the PLL is utilized, the CPN is hence a mixture of two VCO modules: the VCO modules and the reference oscillator modules. The VCO functions at high frequencies whereas the reference oscillator is usually works at low frequencies. In practice, the effect of the reference oscillator CPN is ignored since it could be filtered. Thus, to decrease the effect of the

VCO phase noise, a low-pass PLL filter $F_B(z)$ is used in a closed-loop case. Consequently, in an open-loop scenario, the Wiener phase noise is filtered by a high-pass filter $F(z) = 1 - F_B(z)$. At the output of the PLL, the filtered phase noise PSD is:

$$S_\theta(f) = S_\varepsilon(f).|F(z)|^2 \quad (26)$$

The open-loop PLL synthesizer is characterized by a second order filter whose coefficients are synthesized according to the resonance parameter and the cut-off. It is written as:

$$F(z) = \frac{b_0 + b_1 z^{-1} + b_2 z^{-2}}{a_0 + a_1 z^{-1} + a_2 z^{-2}} \quad (27)$$

4.2. MIMO-SCMA-OFDM Model

In this section, a generalized framework describing an SCMA-OFDM system subject to the CPN is presented. Figure 15 shows a MIMO-SCMA-OFDM transmitter/receiver chain for a downlink communication with N_u users.

For each user m, information bits b_m are fed directly to a sparse code multiple access encoder module which assigns B bits for each of the complex SCMA codeword $\boldsymbol{a}^m$. Therefore, each complex symbol is spread over N_F resource blocks, which is equal to the spreading factor. Using an IFFT of N sub-carriers, every user m transmits $U = N/N_F$ data complex symbols $\boldsymbol{c}^m$ of the m^{th} user on the i^{th} SCMA-OFDM, it is selected from the SCMA codebook of the m^{th} user; $\boldsymbol{V}^m$is a matrix that maps non-zero dimensions of the codeword to the N_F –dimensional complex domain. For simplicity and without loss of generality, we will remove the index "i" from the results.

The transmitted symbol of the m^{th} user over one resource block from antenna “TX” is expressed as:

$$c_{q,s}^{m,TX} = \boldsymbol{v}_q^{m,TX} \times \boldsymbol{a}_s^{m,TX} \tag{28}$$

For a given constellation point, s could be omitted, hence we can write:

$$c_q{}^{m,TX} = \boldsymbol{v}_q^{m,TX} \times \boldsymbol{a}^{m,TX} \tag{29}$$

where $q = 0, \dots, N_F - 1$ is the index of the resource block.

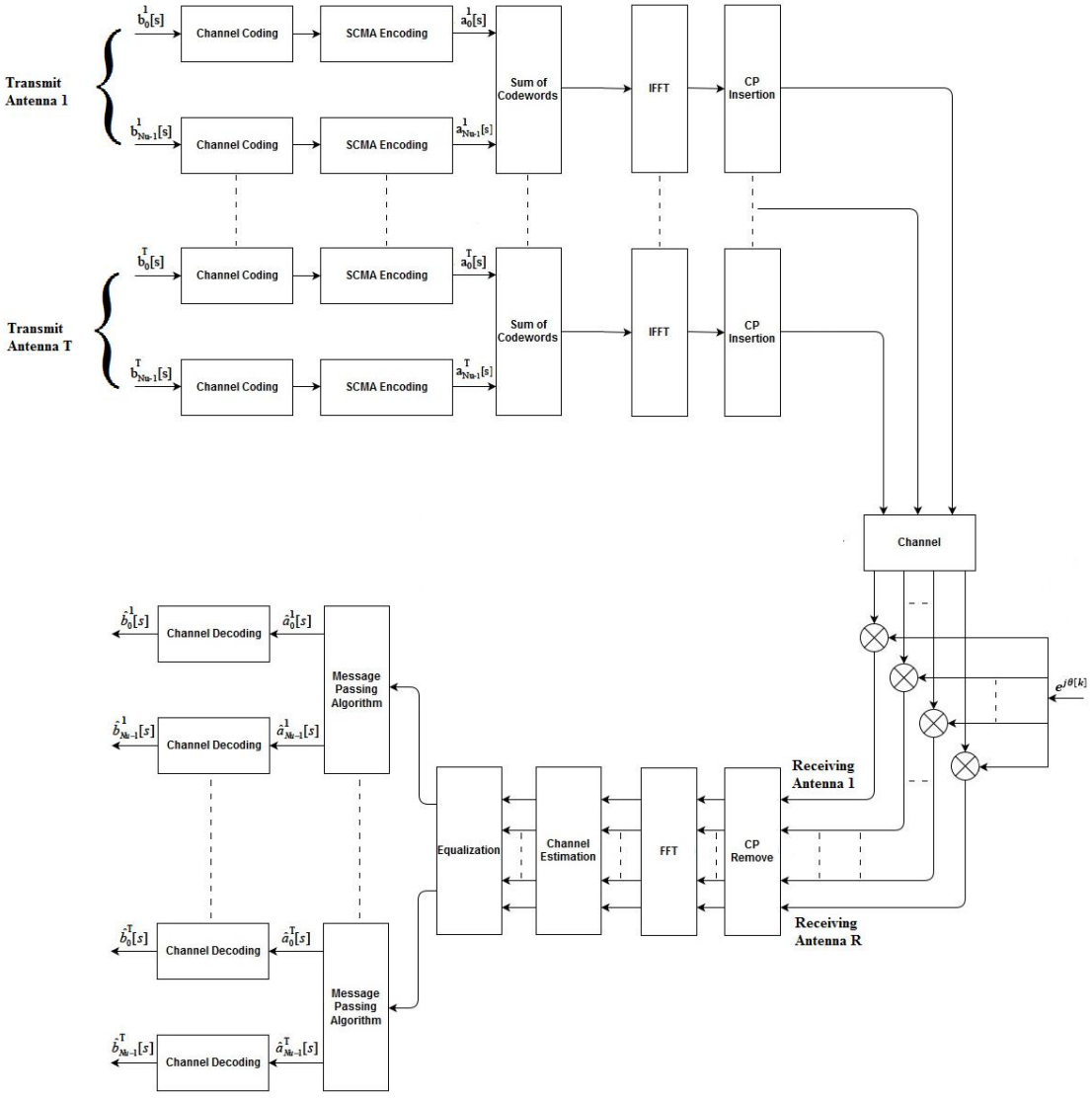

Fig. 15: MIMO-SCMA-OFDM Block Diagram

The data of all users are added together; hence, the output of all users could be given by:

$$d_q^{TX} = \sum_{m=0}^{N_u-1} {c_q}^{m,TX} = \sum_{m=0}^{N_u-1} \boldsymbol{v}_q^{m,TX} \times \boldsymbol{a}^{m,TX} \tag{30}$$

If we want to add a power allocation factor per resource block, we get

$$d_q^{TX} = \sum_{m=0}^{N_u-1} \sqrt{P_q^{m,TX}}.\boldsymbol{v}_q^{m,TX}.\boldsymbol{a}^{m,TX} \tag{31}$$

The signal at the IFFT output is:

$$x^{TX}(k) = \sum_{u=0}^{U-1} \sum_{q=0}^{N_F-1} d_q^{TX}[u].e^{\frac{j2\pi(uN_F+q)k}{N}} \tag{32}$$

$d_q^{TX}[u]$ is simply d_q^{TX}but for OFDM sub band u.

At the output of the IFFT, a cyclic prefix (CP) of v samples is added to remove the inter symbol interference (ISI). The complex signal is then upconverted to the carrier frequency by the radio frequency (RF) unit. It is afterward convoluted by the multipath propagation channel, which is characterized by its base band function as FIR $h\,(z) = \sum_{k=0}^{L-1} g[k]z^{-k}$. $g[k]$ is the channel impulse response (CIR) and L is the delay spread which is presumed less than the cyclic prefix ($L \leq v$). The signal at the channel output is then degraded by an AWGN with zero mean and variance equal to σ^2. At the receiver, the signal is downconverted by the receiver RF unit. The CPN is represented in this paper as the phase error between the CPN at transmitter and that at the receiver. It can be modeled by a random phase rotation of the samples at the input of CP remove unit. Thus, the received samples on the antenna "RX" can be expressed as:

$$r_p^{RX}[w] = r^{RX}[wN_F + p]$$
$$= \sum_{t=1}^{T} \sum_{u=0}^{U-1} \sum_{q=0}^{N_F-1} d_q^t[u] \Phi^{RX,t}(u, w, q, p) + n^{RX}[uN_F + q] \quad (33)$$

Where the equivalent channel transfer function including IFFT, CIR, FFT and CPN is given by:

$$\Phi^{RX,t}(u, w, q, p) = \frac{h^{RX,t}[uN_F + q]}{N} \sum_{k=0}^{N-1} e^{-j2\pi \frac{(u-w)N_F + (q-p)}{N} k} e^{j\theta[k]} \quad (34)$$

$d_q^t[u] = d^t[uN_F + q]$, and $h[uN_F + q] = h(z)|_{z=e^{j2\pi \frac{uN_F+q}{N}}}$, is the FFT of the CIR $g[k]$ on the sub-carrier q of the u^{th} sub band, $N[k]$ is the AWGN and $\theta[k]$ is the CPN.

$d_q^t[u] = d^t[uN_F + q]$, and $h[uN_F + q]$ is the time-domain channel coefficient on the sub-carrier q of the u^{th} sub band, $N[k]$ is the AWGN and $\theta[k]$ is the CPN.

Equation (12) shows that for $w = u$ and $p = q$, $\Phi(u, w, q, p)$ represents the common phase error (CPE) modifying equally the signal transmitted on each sub-carrier. Practically, the CPE is predicted simultaneously with the frequency channel coefficients and adjusted by the equalizer.

At the output of the FFT module, the signal carried by the $(wN_F + p)^{th}$ sub-carrier of the i^{th} OFDM symbol is:

$$r^{RX}[wN_F + p] = \frac{1}{N} \sum_{t=1}^{T} \sum_{u=0}^{U-1} \sum_{q=0}^{N_F-1} d^t[uN_F + q] h^{RX,t}[uN_F + q] \sum_{k=0}^{N-1} e^{-j2\pi \frac{(u-w)N_F + (q-p)k}{N}} e^{j\theta[k]} + n^{RX}[uN_F + q]$$

$$= \frac{1}{N}\sum_{t=1}^{T}\sum_{u=0}^{U-1}\sum_{q=0}^{N_F-1}\sum_{m=0}^{N_u-1}\sqrt{P^{m,t}[uN_F+q]}h^{RX,t}[uN_F+q]\boldsymbol{v}_q^{m,t}\,\boldsymbol{a}_u^{m,t}\sum_{k=0}^{N-1}e^{-j2\pi\frac{(u-w)N_F+(q-p)k}{N}}\,e^{j\theta[k]} \quad (35)$$
$$+n^{RX}[uN_F+q]$$

Without loss of interest, let us assume that we are interested in reference user 0, hence we can write:

$$r^{0,RX}[wN_F+p] = \frac{1}{N}\sum_{t=1}^{T}\sum_{u=0}^{U-1}\sum_{q=0}^{N_F-1}\sqrt{P^{0,t}[uN_F+q]}\boldsymbol{v}_q^{0,t}\boldsymbol{a}_u^{0,t}\Phi^{RX,t}(u,w,q,p) +$$
$$\frac{1}{N}\sum_{t=1}^{T}\sum_{m=1}^{N_u-1}\sum_{u=0}^{U-1}\sum_{q=0}^{N_F-1}\sqrt{P^{m,t}[uN_F+q]}\boldsymbol{v}_q^{m,t}\boldsymbol{a}_u^{m,t}\Phi^{RX,t}(u,w,q,p) + n^{RX}[uN_F+q]$$
$$= \frac{1}{N}\sum_{t=1}^{T}\sqrt{P^{0,t}[wN_F+p]}\;\boldsymbol{v}_p^{0,t}\boldsymbol{a}_w^{0,t}\Phi^{RX,t}(w,w,p,p) \quad (36)$$
$$+\frac{1}{N}\sum_{t=1}^{T}\sum_{q=0}^{N_F-1}\sqrt{P^{0,t}[wN_F+q]}\boldsymbol{v}_q^{0,t}\boldsymbol{a}_w^{0,t}\Phi^{RX,t}(w,w,q,p)$$
$$+\frac{1}{N}\sum_{t=1}^{T}\sum_{\substack{u=0\\u\neq w}}^{U-1}\sum_{q=0}^{N_F-1}\sum_{m=1}^{N_u-1}\sqrt{P^{m,t}[uN_F+q]}\boldsymbol{v}_q^{m,t}\boldsymbol{a}_u^{m,t}\Phi^{RX,t}(u,w,q,p) + n^{RX}[wN_F+p]$$

After equalization by $Z[wN_F+p]$:

$$y^{TX}[wN_F+p] = \sum_{r=1}^{R}Z^{r,TX}[wN_F+p].r^{r}[wN_F+p] \quad (37)$$

$Z[wN_F+p]$ should equalize $h_{eq}[wN_F+p]$. It is given by:

$$h_{eq}[wN_F+p] = \Phi(w,w,p,p) \quad (38)$$

Let $r[wN_F] = \begin{bmatrix} r(wN_F) \\ r(wN_F+1) \\ \vdots \\ r(wN_F+N_F-1) \end{bmatrix}$ it is a vector of size $(N_F \times 1)$

And let us focus on user 0.

Let $\boldsymbol{V}^{0,T} = \begin{bmatrix} 0 & 1 & 0 & 0 \\ 0 & 0 & 0 & 1 \end{bmatrix} = \begin{bmatrix} \boldsymbol{v}^{0,T,1} \\ \boldsymbol{v}^{0,T,2} \end{bmatrix}$ (For $N_F = 4\ and\ W = 2$)

Then, we need to multiply $\boldsymbol{V}^{0,T}$ by $R[wN_F]$; this will give us two elements, each corresponding to one row vector. (Matrices are defined in Appendix A)

We are interested in estimating the first part of the transmitted symbol in the w^{th} sub-band and p^{th} subcarrier considering that the same data is transmitted on all the antennas. The estimated transmitted symbol can be written as:(see Appendix B for calculations)

$$\hat{a}_{1,w}^{TX} = \sum_{p=0}^{N_F-1} \boldsymbol{v}_p^{0,1,T,TX} y^{TX}[wN_F + p] = A + B + C + D \tag{39}$$

The terms $A, B, C,$ and D can also be written as

$$A = \sum_{r=1}^{R}\sum_{t=1}^{T} \boldsymbol{v}^{0,1,T,TX}.\boldsymbol{Z}^{r,TX}[w].\boldsymbol{\Psi}^{rt}[w,w].\boldsymbol{P}^{0,t}[w].\boldsymbol{v}^{0,1,t}.a_w^{0,t}$$

$$B = \sum_{r=1}^{R}\sum_{t=1}^{T} \boldsymbol{v}^{0,1,T,TX}.\boldsymbol{Z}^{r,TX}[w].\boldsymbol{\Psi}^{rt}[w,w].\boldsymbol{Q}^{t}[w].\boldsymbol{U}^{t}[w]\,.\boldsymbol{a}_w^t$$

$$C = \sum_{r=1}^{R}\sum_{t=1}^{T}\sum_{\substack{u=0 \\ u\neq w}}^{U-1} \boldsymbol{v}^{0,1,T,TX}.\boldsymbol{Z}^{r,TX}[w].\boldsymbol{\Psi}^{rt}[w,u].\boldsymbol{Q}^{t}[u].\boldsymbol{U}^{t}[u]\,.\boldsymbol{a}_u^t \tag{40}$$

$$= \sum_{r=1}^{R}\sum_{t=1}^{T} \boldsymbol{v}^{0,1,T,TX}.\boldsymbol{Z}^{r,TX}[w].\boldsymbol{\Psi}^{rt}[w,s].\boldsymbol{Q}^{t}[u].\boldsymbol{U}^{t}[u]\,.\boldsymbol{a}_u^t$$

$$D = \sum_{r=1}^{R} \boldsymbol{v}^{0,1,T,TX}.\boldsymbol{Z}^{r,TX}[w].\boldsymbol{n}^{r}[w]$$

A denotes the useful signal, B the multiple access interference (MAI) signal within sub-band w,C the interference created by all the users from other sub-bands (IBI), and D is the noise.

Therefore, the estimated transmitted symbol in the w^{th} sub-band and p^{th} subcarrier can be written as:

$$\begin{aligned}\hat{a}_{1,w} &= \sum_{r=1}^{R}\sum_{t=1}^{T} \boldsymbol{v}^{0,1,T,TX}.\boldsymbol{Z}^{r,TX}[w].\boldsymbol{\Psi}^{rt}[w,w].\boldsymbol{P}^{0,t}[w].\boldsymbol{V}^{0,t}.a_w^{0,t} \\ &+ \sum_{r=1}^{R}\sum_{t=1}^{T} \boldsymbol{v}^{0,1,T,TX}.\boldsymbol{Z}^{r,TX}[w].\boldsymbol{\Psi}^{rt}[w,w].\boldsymbol{Q}^{t}[w].\boldsymbol{U}^{t}[w]\,.\boldsymbol{a}_w^{t} \\ &+ \sum_{r=1}^{R}\sum_{t=1}^{T}\sum_{\substack{u=0\\u\neq w}}^{U-1} \boldsymbol{v}^{0,1,T,TX}.\boldsymbol{Z}^{r,TX}[w].\boldsymbol{\Psi}^{rt}[w,u].\boldsymbol{Q}^{t}[u].\boldsymbol{C}^{t}[u]\,.\boldsymbol{a}_u^{t} \\ &+ \sum_{r=1}^{R} \boldsymbol{v}^{0,1,T,TX}.\boldsymbol{Z}^{r,TX}[w].\boldsymbol{n}^{r}[w] \end{aligned} \tag{41}$$

$$\begin{aligned}&= \sum_{r=1}^{R}\sum_{t=1}^{T} \boldsymbol{v}^{0,1,T,TX}.\boldsymbol{Z}^{r,TX}[w].\boldsymbol{\Psi}^{rt}[w,w].\boldsymbol{P}^{0,t}[w].\boldsymbol{V}^{0,t}.\boldsymbol{a}_w^{0,t} \\ &+ \sum_{r=1}^{R}\sum_{t=1}^{T} \boldsymbol{v}^{0,1,T,TX}.\boldsymbol{Z}^{r,TX}[w].\boldsymbol{\Psi}^{rt}[w,w].\boldsymbol{Q}^{t}[w].\boldsymbol{U}^{t}[w]\,.\boldsymbol{a}_w^{t} \\ &+ \sum_{r=1}^{R}\sum_{t=1}^{T} \boldsymbol{v}^{0,1,T,TX}.\boldsymbol{Z}^{r,TX}[w].\boldsymbol{\Psi}^{rt}[w,s].\boldsymbol{Q}^{t}[u].\boldsymbol{C}^{t}[u]\,.\boldsymbol{a}_u^{t} \\ &+ \sum_{r=1}^{R} \boldsymbol{v}^{0,1,T,TX}.\boldsymbol{Z}^{r,TX}[w].\boldsymbol{n}^{r}[w] \end{aligned}$$

4.3. Analytical SINR Evaluation

4.3.1. Properties of Random Matrix and Free Probability Theory

Property 1: if a matrix **A** is a (*NF*, *NF*) uniformly bounded deterministic matrix and $\boldsymbol{v_m} = \left[v_0^m, \ldots, v_{N_F-1}^m\right]$ where v_l^m have zero mean, unit variance, then:

$$\boldsymbol{v_m^H A v_m} \xrightarrow{\boldsymbol{N_F\to\infty}} trace(\boldsymbol{A}) \tag{42}$$

Property 2: if the matrices $\boldsymbol{V}[w]\boldsymbol{CV^H}[w]$ and $\boldsymbol{Z}[w]\boldsymbol{\Psi}[w]\boldsymbol{\Psi^H}[w]\boldsymbol{Z^H}[w]$ are symptotically free almost everywhere. Based on this freedom, one can conclude:

$$trace(\boldsymbol{Z}[w]\boldsymbol{\Psi}[w]\boldsymbol{V}[w]\boldsymbol{CV^H}[w]\boldsymbol{\Psi^H}[w]\boldsymbol{Z^H}[w]) \xrightarrow{N_F\to\infty} trace(\boldsymbol{Z}[w]\boldsymbol{\Psi}[w]\boldsymbol{\Psi^H}[w]\boldsymbol{Z^H}[w]) \times trace(\boldsymbol{V}[w]\boldsymbol{CV^H}[w]) \quad (43)$$

4.3.2. SINR Expressions in Rayleigh Channel Model

The SINR for each sub-band *w* for one channel realization, so-called instantaneous SINR, is obtained from (41) by computing the variances over A, B, Cand D. Since the symbols transmitted over all the sub-bands are independent and uncorrelated; thus, the different interference components will become uncorrelated as well. Therefore, the SINR can be expressed as:

$$\boxed{SINR = \frac{E[|A|^2]}{E[|B|^2] + E[|C|^2] + E[|D|^2]}} \quad (44)$$

The expectations values in (44) are given by: (see calculations in Appendix C)

$$E[|A|^2] = T.R.W$$

$$E[|B|^2] = W.(N_u - 1).\sum_{r=1}^{R}\sum_{t=1}^{T}\sum_{p=0}^{N_F-1}\left|\gamma\sum_{q=0}^{N_F-1}\frac{h^{r,t}[wN_F+q]\ \sum_{k=0}^{N-1}e^{-\frac{j2\pi(p-q)k}{N}}e^{j\theta[k]}}{h^{r,TX}[wN_F+p]\ \sum_{v=0}^{N-1}e^{j\theta[v]}}\right|^2$$

$$E[|C|^2] = W.N_u\sum_{r=1}^{R}\sum_{t=1}^{T}\sum_{p=0}^{N_F-1}\sum_{\substack{u=0\\u\neq w}}^{U-1}\left|\sum_{\boldsymbol{q=0}}^{N_F-1}\frac{h^{r,t}[uN_F+q]\ \sum_{k=0}^{N-1}e^{-\frac{j2\pi k((w-u)N_F+(p-q))}{N}}e^{j\theta[k]}}{h^{r,TX}[wN_F+p]\ \sum_{v=0}^{N-1}e^{j\theta[v]}}\right|^2 \quad (45)$$

$$E[|D|^2] = \frac{\sigma^2}{N_F}\sum_{r=1}^{R}\sum_{p=0}^{N_F-1}\left|\frac{1}{h^{r,TX}[wN_F+p].CPE}\right|^2$$

4.3.3. SINR Expressions in AWGN Channel Model

The expectations values in (44) are given by: (see calculations in Appendix C)

$$E[|A|^2] = T.R.W$$

$$E[|B|^2] = W.(N_u - 1).T.R.\sum_{p=0}^{N_F-1}\left|\gamma\sum_{q=0}^{N_F-1}\frac{\sum_{k=0}^{N-1} e^{-\frac{j2\pi(p-q)k}{N}} e^{j\theta[k]}}{\sum_{v=0}^{N-1} e^{j\theta[v]}}\right|^2$$

$$E[|C|^2] = W.N_u.T.R.\sum_{p=0}^{N_F-1}\sum_{\substack{u=0\\u\neq w}}^{U-1}\left|\sum_{\boldsymbol{q=0}}^{N_F-1}\frac{\sum_{k=0}^{N-1} e^{-\frac{j2\pi k((w-u)N_F+(p-q))}{N}} e^{j\theta[k]}}{\sum_{v=0}^{N-1} e^{j\theta[v]}}\right|^2 \quad (46)$$

$$E[|D|^2] = \frac{\sigma^2.R}{|CPE|^2}$$

4.4. Results

In this section, the analytical and simulation results of the MIMO-SCMA-OFDM scheme are provided. The parameters for the analytical and simulation results are given in TABLE 2 and TABLE 3 respectively.

4.4.1. Analytical Results

Table 2: Parameters for Analytical MIMO-SCMA-OFDM System

Parameters	Values
Number of Resource Blocks (N_F)	6, 15
Number of Layers (Nu)	4, 6
Overloading Factor (Nu/N_F)	150%, 250%

Modulation	QPSK
Cyclic Prefix Length	256
Diffusion Factor	1Hz, 10Hz, 100Hz, 1kHz, 10kHz, 100kHz, 1MHz
Channel	Rayleigh, AWGN
Noise Variance	0, 0.001, 0.0032, 0.01, 0.0316, 0.1
Gamma factor (100% - MPA performance)	0, 0.01, 0.02, 0.03, 0.04, 0.05

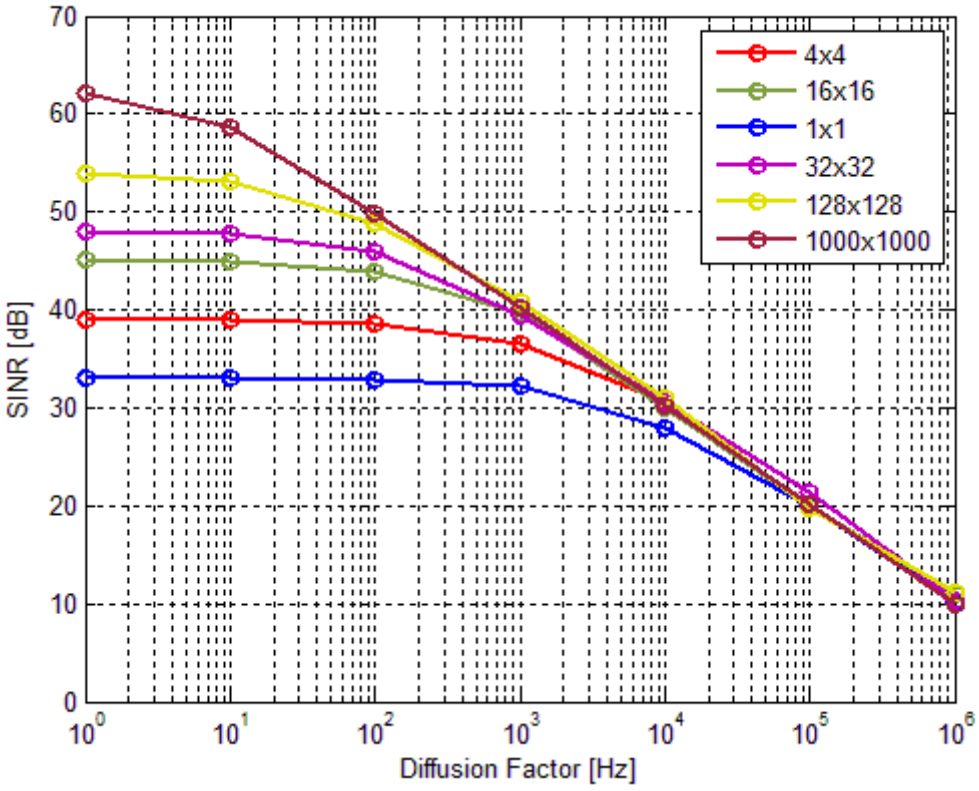

Fig. 16: MIMO-SCMA-OFDM, N_u=6 N_F=4 gamma=0, variance=0.001, AWGN channel

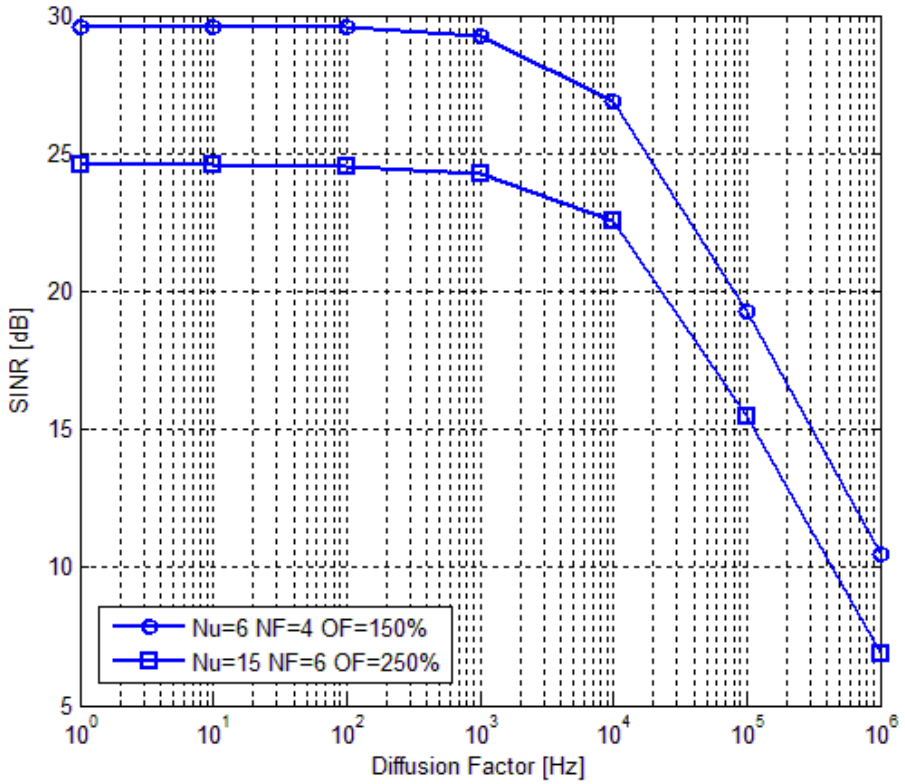

Fig. 17: SISO-SCMA-OFDM, gamma=0.01, variance=0.001, AWGN channel

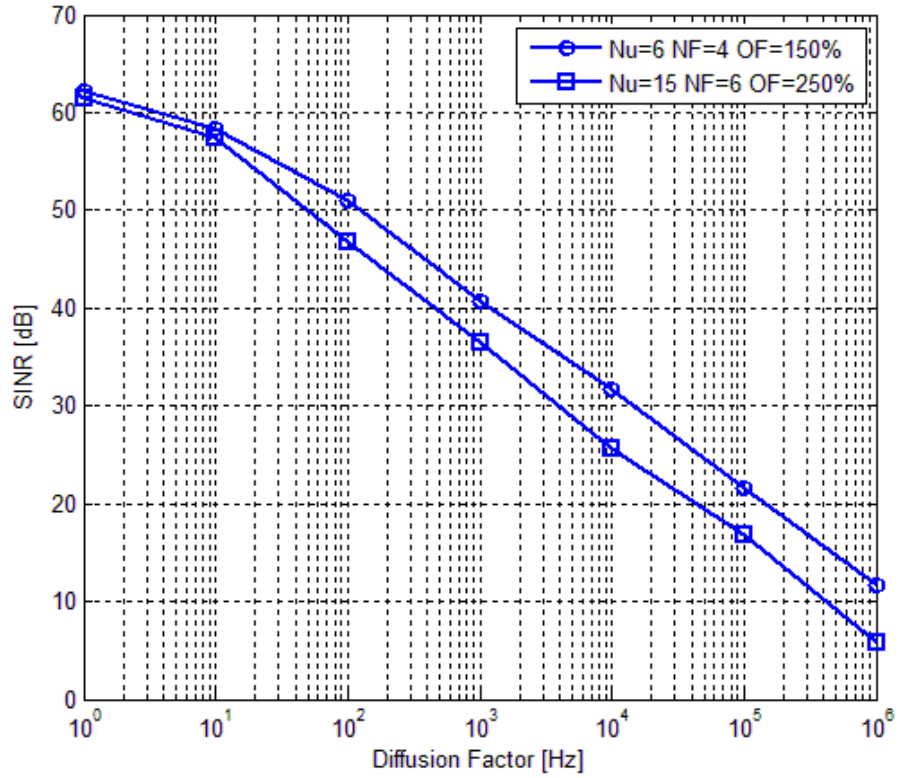

Fig. 18: massive MIMO-SCMA-OFDM, gamma=0, variance=0.001, AWGN channel

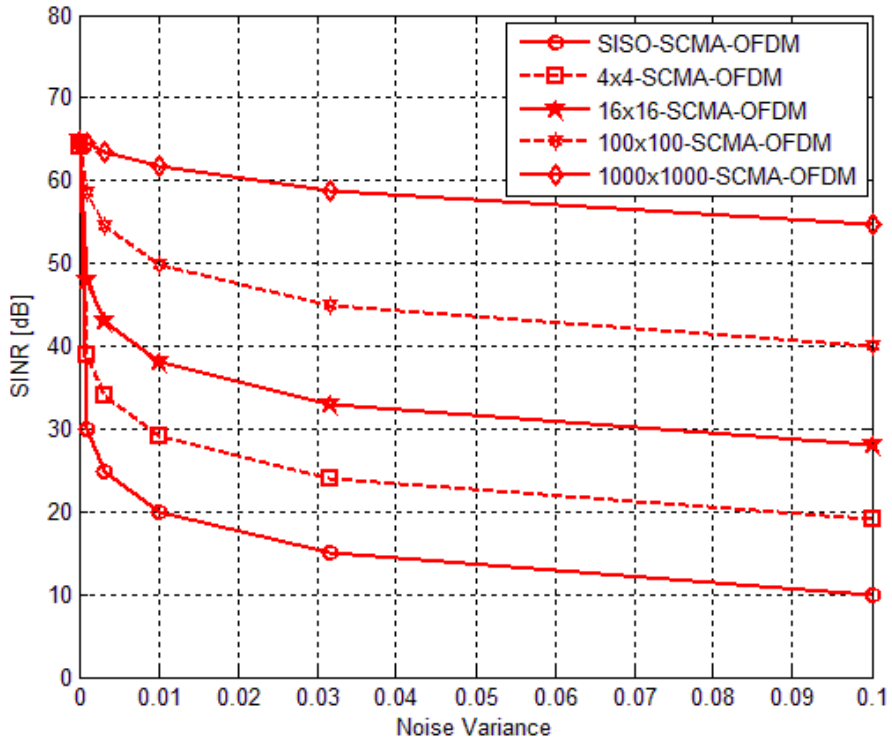

Fig. 19: MIMO-SCMA-OFDM, Diffusion Factor=1Hz, gamma= 0, N_u=6, N_F=4, AWGN channel

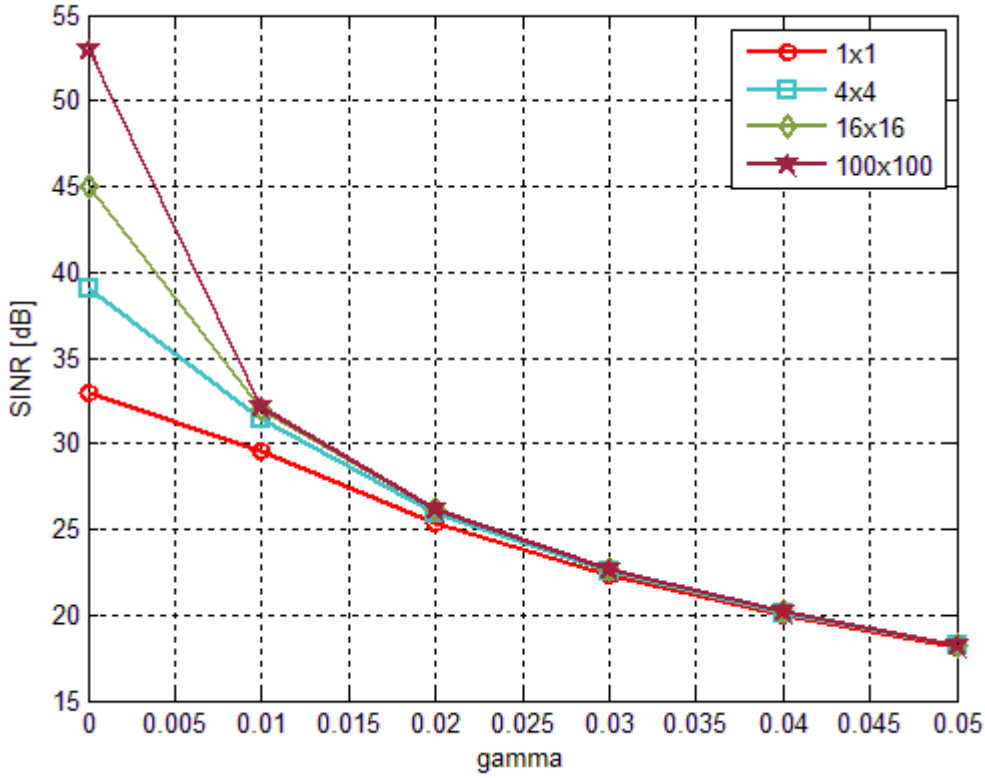

Fig. 20: MIMO-SCMA-OFDM, Diffusion Factor=1 Hz, Nu=6, N_F=4, variance=0.001, AWGN Channel

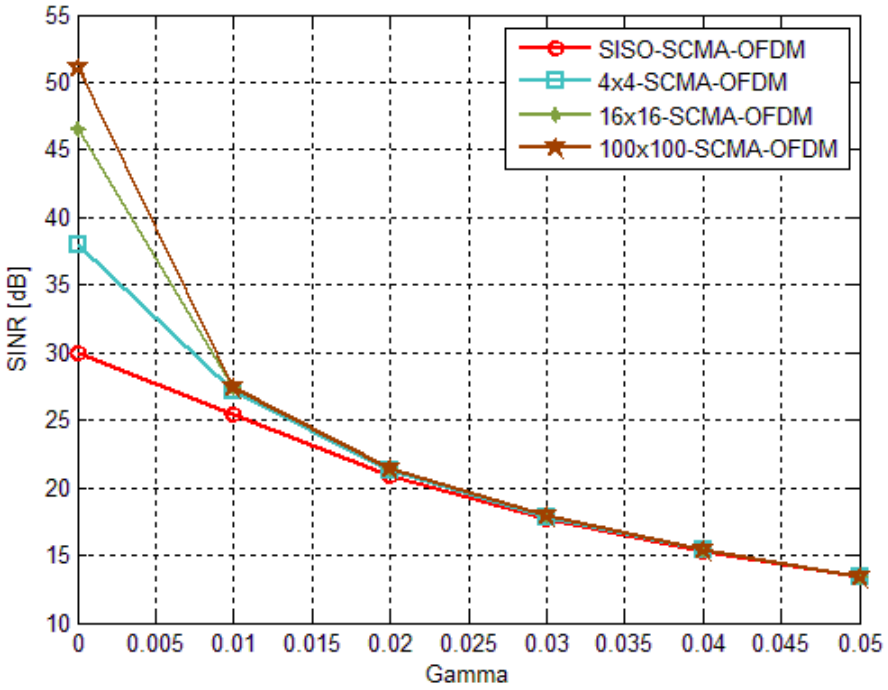

Fig. 21: MIMO-SCMA-OFDM, Diffusion Factor=1 Hz, Nu=6, N_F=4, variance=0.001, Rayleigh Channel

4.4.2. Simulation Results

Table 3: Simulation Parameters for MIMO-SCMA-OFDM System

Simulation Parameters	Values
Number of Resource Blocks (N_F)	4
Number of Layers (Nu)	6
Overloading Factor (Nu/N_F)	1.5
Modulation	QPSK
Cyclic Prefix Length	256
Diffusion Factor	1Hz, 10Hz, 100Hz, 1kHz, 10kHz, 50kHz, 100kHz, 1MHz
Channel	Rayleigh, AWGN

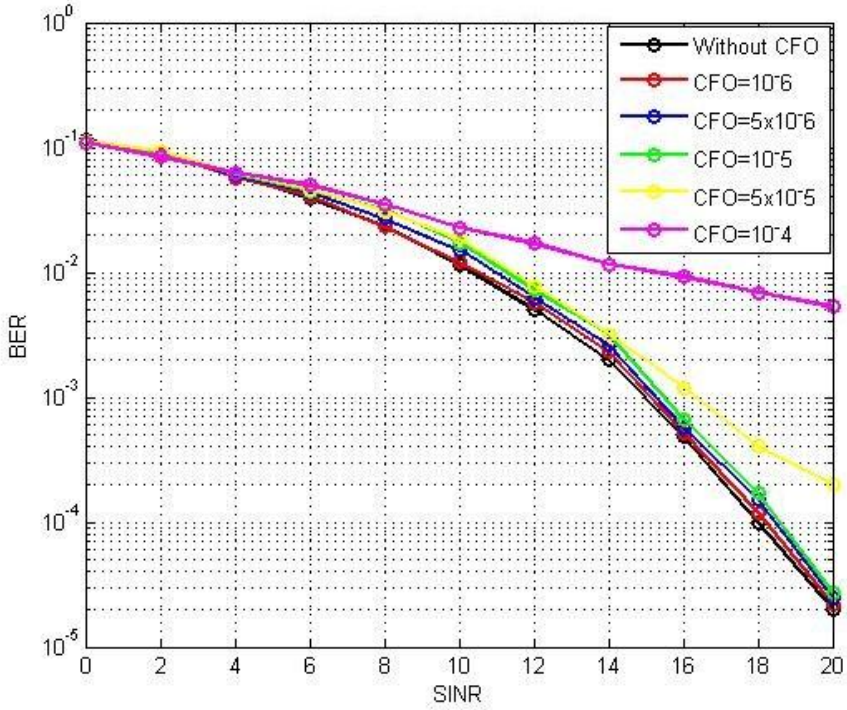

Fig. 22: Uncoded SISO-SCMA-OFDM, QPSK modulation, ZF-Equalization, AWGN channel

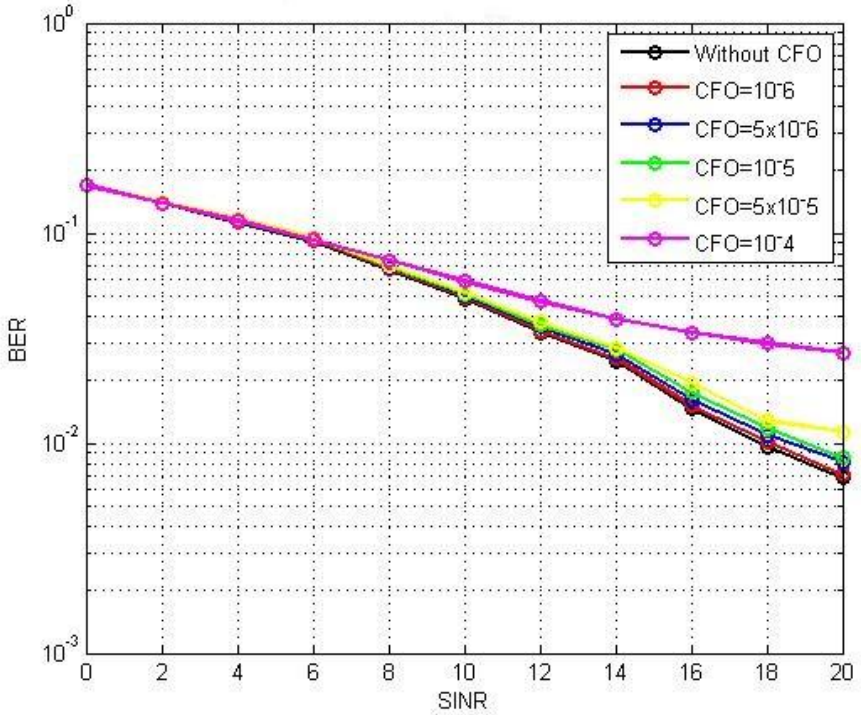

Fig. 23: Uncoded SISO-SCMA-OFDM, QPSK modulation, ZF-Equalization, Rayleigh channel

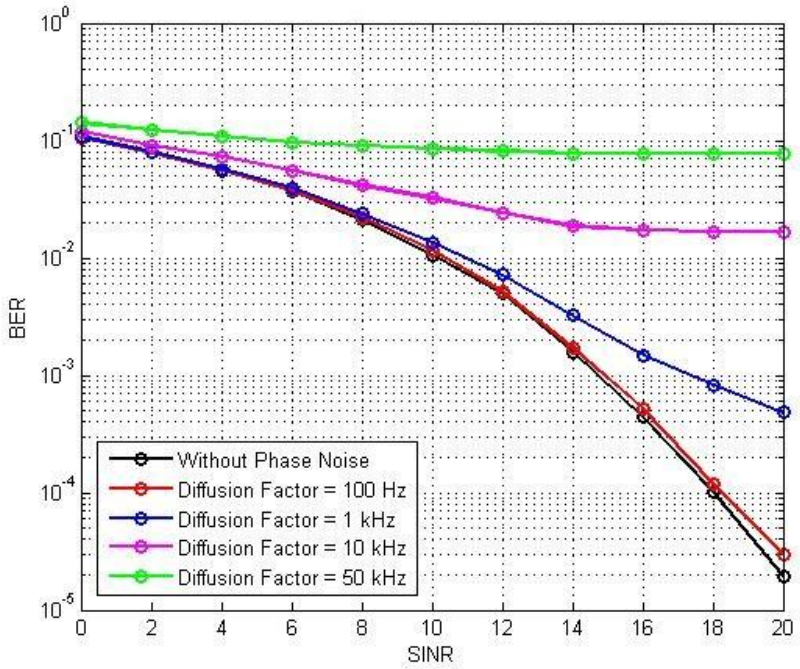

Fig. 24: Uncoded SISO-SCMA-OFDM, QPSK modulation, ZF-Equalization, AWGN channel

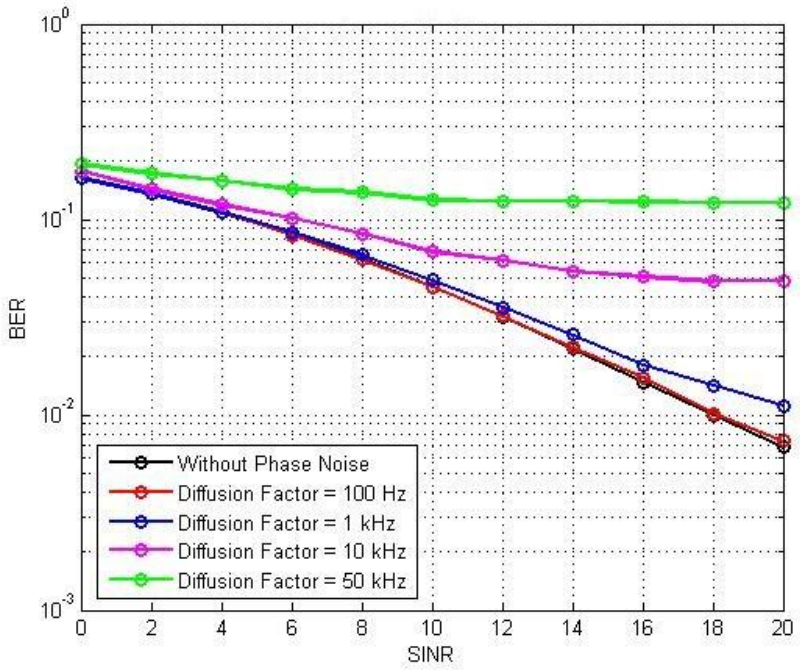

Fig. 25: Uncoded SISO-SCMA-OFDM, QPSK modulation, ZF-Equalization, Rayleigh channel

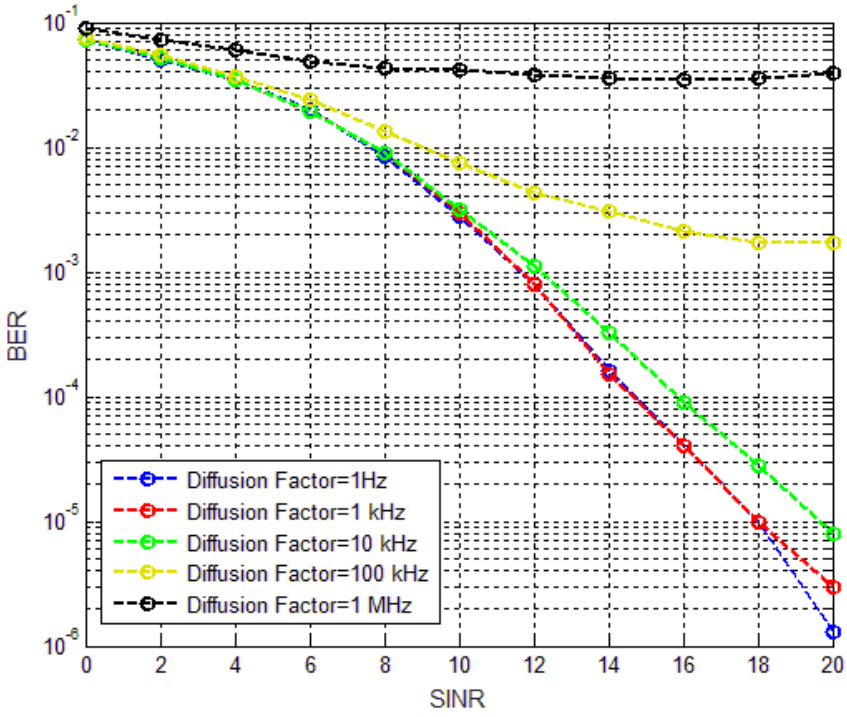

Fig. 26: Uncoded 2x2-SCMA-OFDM, QPSK modulation, ML-Detection, AWGN channel

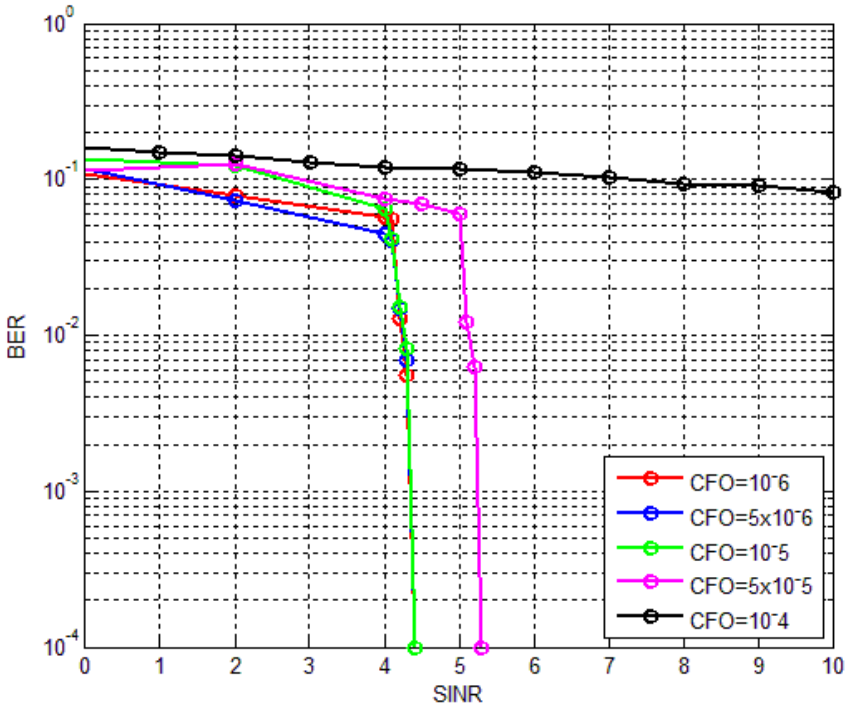

Fig. 27: Turbo coded 2x2-SCMA-OFDM, rate=1/3 QPSK modulation, Rayleigh channel

4.5. Results Analysis

In Figure 16, we show the SINR performance with respect to different diffusion factors in SISO, MIMO-SCMA-OFDM systems. It is realized that MIMO has a superior performance over SISO for diffusion factor less than 10kHz. But above this value they almost have the same performance and it is recommendable to use SISO or a very small number of antennas and saving power and complexity for the same performance. It is also realized that the performance of SISO is stable for small diffusion factor less than 1kHz, after that the performance starts to degrade; on the other hand, we see that MIMO performance degrades from the beginning in almost a linear manner.

In Figure 17, we compared between two SISO-SCMA-OFDM systems; the first had an overloading factor of 150% and the second had an overloading factor of 250%, it is shown that the first system outperform the second one; but their degradation is in the same way, the both are stable for a diffusion factor less than 1kHz and they degrade after that.

In Figure 18, we had two Massive MIMO-SCMA-OFDM systems with same overloading factors as in Figure 17. We can see that due to the effect of high number of antennas and the effect of gamma, the two systems had a closer performance than in Figure 17; they almost had the same performance for a very small diffusion factor.

In Figure 19, we studied the SINR performance of SISO and MIMO-SCMA-OFDM systems with respect to the noise variance; it is illustrated the with the increase of the number of antennas the system become more and more robust again the effect of the noise. For example, when the noise variance is increased from 0 to 0.01 the SINR of SISO-SCMA-OFDM decrease 45db while the SINR of 1000x1000-SCMA-OFDM system decrease only 3db.

Figures 20 and 21 display the huge effect of the MPA performance in the system, when this performance decrease by 1% only the SINR degrades drastically. So it is shown that when we have 99% and less of the MPA performance, no increase in the number of antennas is able to boost the SINR performance and in this case it is better to use SISO and have the same performance as MIMO.

Figure 22 to 27 are the simulation results; they came in line with the analytical results. So it is realized that in Figures 22,23 and 27 the CFO has a negligible effect on the system when it is less than 10^{-4}; after that value BER performance degrades rapidly. The same is illustrated in Figures 24 and 25, where a small Diffusion factor (< 10kHz) has a negligible effect on the BER performance of the system, while after this value starts the system performance degradation.

CHAPTER 5

CONCLUSION AND FUTURE WORK

In the first part of the thesis, we developed a MIMO-SCMA system and we evaluated its performance in terms of the bit error rate for different channels, modulation schemes, and equalization techniques.

In the second part of the thesis, the MIMO-SCMA system became a MIMO-SCMA-OFDM system in order to model the effects of carrier frequency offset and carrier phase noise on the MIMO-SCMA system. Furthermore, using some properties of random matrix and free probability theory, we were able to develop a new analytical expression of the SINR in an asymptotic regime.

As for future work, the MIMO-SCMA and the MIMO-SCMA-OFDM system will be studied in terms of throughput and energy efficiency. Moreover, using asymptotic SINRs, the SINR degradations and new weighting functions will be derived. Finally, using exponential effective SINR mapping (EESM), the bit error rate (BER) at the output of the channel decoder will be predicted.

APPENDIX A

In order to write the received signal with matrix-vector notation, the following matrices are defined:

- $\boldsymbol{Z}[w] = diag(Z[wN_F], \dots, Z[wN_F + N_F - 1])$ is the $N_F \times N_F$ diagonal matrix which equalizes the diagonal elements of the channel matrix $H[w, u]$.
- $\boldsymbol{n}[w] = \left[N[wN_F], \dots, N[wN_F + N_F - 1]\right]^T$ is the $N_F \times 1$ AWGN with mean equal 0 and variance σ^2.
- $\boldsymbol{V}^0 = \left[\boldsymbol{v}_0^{0,T}, \dots, \boldsymbol{v}_{N_F-1}^{0,T}\right]^T$, where V^0 is of size $N_F \times W$.
- $\boldsymbol{a}_w^0 = \begin{pmatrix} b_1 \\ \vdots \\ c_1 \end{pmatrix} or \begin{pmatrix} b_2 \\ \vdots \\ c_2 \end{pmatrix} or \begin{pmatrix} b_3 \\ \vdots \\ c_3 \end{pmatrix} or \dots or \begin{pmatrix} b_M \\ \vdots \\ c_M \end{pmatrix}$, it is of size $W \times 1$ where M is the constellation size.
- $\boldsymbol{a}_w = \left(\boldsymbol{a}_w^1, \dots, \boldsymbol{a}_w^{N_u-1}\right)^T$.
- $\boldsymbol{a}_u = \left(\boldsymbol{a}_u^0, \dots, \boldsymbol{a}_u^{N_u-1}\right)^T$.
- $\boldsymbol{U}[w] = \begin{pmatrix} \boldsymbol{v}_0^1 & \boldsymbol{v}_0^{2,} & \boldsymbol{v}_0^{N_u-1} \\ \boldsymbol{v}_1^1 & \boldsymbol{v}_1^2 & \dots \ \boldsymbol{v}_1^{N_u-1} \\ \vdots & \vdots & \vdots \\ \boldsymbol{v}_{N_F-1}^1 & \boldsymbol{v}_{N_F-1}^2 & \boldsymbol{v}_{N_F-1}^{N_u-1} \end{pmatrix}$, $\boldsymbol{U}[w]$ is of size $N_F \times \left(W(N_u - 1)\right)$, it is the matrix including the $\boldsymbol{V}$ matrices of all the other users
- $\boldsymbol{C}[u] = \begin{pmatrix} \boldsymbol{v}_0^0 & \boldsymbol{v}_0^1 & \boldsymbol{v}_0^{N_u-1} \\ \boldsymbol{v}_1^0 & \boldsymbol{v}_1^1 & \dots \ \boldsymbol{v}_1^{N_u-1} \\ \vdots & \vdots & \vdots \\ \boldsymbol{v}_{N_F-1}^0 & \boldsymbol{v}_{N_F-1}^1 & \boldsymbol{v}_{N_F-1}^{N_u-1} \end{pmatrix}$, $\boldsymbol{C}[u]$is of size $N_F \times 2N_u$, it is the matrix including the $\boldsymbol{V}$ matrices of all the users.
- $\boldsymbol{P}^0[w] = diag\left(\sqrt{P_0^0}, \dots, \sqrt{P_{N_F-1}^0}\right)$, is the $N_F \times N_F$ diagonal matrix which entries are the signal amplitudes allocated to each resource block for user 0.

- $\boldsymbol{Q}\,[w] = \begin{pmatrix} \sqrt{P_0^1} & \sqrt{P_0^2} & \sqrt{P_0^{N_u-1}} \\ \vdots & \vdots & \vdots \\ \sqrt{P_{N_F-1}^1} & \sqrt{P_{N_F-1}^2} & \sqrt{P_{N_F-1}^{N_u-1}} \end{pmatrix}$, $\boldsymbol{Q}\,[w]$ is the matrix of size $\big((N_F-1)\times(N_u-1)\big)$ which entries are the signal amplitudes allocated to each resource block for all the users.

- $\boldsymbol{\Psi}[w,w] = \begin{pmatrix} \Phi(w,w,0,0) & \cdots & \Phi(w,w,0,N_F-1) \\ \vdots & \Phi(w,w,p,q) & \vdots \\ \Phi(w,w,N_F-1,0) & \cdots & \Phi(w,w,N_F-1,N_F-1) \end{pmatrix}$

- $\boldsymbol{\Psi}[w,s] = \begin{pmatrix} \boldsymbol{A}[w,0] \\ \boldsymbol{A}[w,1] \\ \vdots \\ \boldsymbol{A}[w,u]_{u\neq w} \\ \vdots \\ \boldsymbol{A}[w,s-1] \end{pmatrix}, with\ \boldsymbol{A}[w,u] = \boldsymbol{\Psi}[w,u]$

- $\boldsymbol{\Psi}[w,u] =$

$$\begin{pmatrix} \Phi(w,u,0,0) & \cdots & \Phi(w,u,0,N_F-1) \\ \vdots & \Phi(w,u,p,q) & \vdots \\ \Phi(w,u,N_F-1,0) & \cdots & \Phi(w,u,N_F-1,N_F-1) \end{pmatrix}$$

APPENDIX B

Solution of Equation (39)

$$\hat{a}_{1,w}^{TX} = \sum_{p=0}^{N_F-1} v_p^{0,1,T,TX} y^{TX}[wN_F + p]$$

$$= \sum_{r=1}^{R}\sum_{t=1}^{T}\sum_{p=0}^{N_F-1}\sum_{u=0}^{U-1}\sum_{q=0}^{N_F-1}\sum_{m=0}^{N_u-1} v_p^{0,1,T,TX} Z^{r,TX}[wN_F + p]\sqrt{P^{m,t}[uN_F + q]}\boldsymbol{v}_q^{m,t}\boldsymbol{a}_u^{m,t}\Phi^{rt}(w,u,p,q)$$

$$= \sum_{r=1}^{R}\sum_{t=1}^{T}\sum_{p=0}^{N_F-1}\sum_{q=0}^{N_F-1} v_p^{0,1,T,TX} Z^{r,TX}[wN_F + p]\sqrt{P^{0,t}[wN_F + p]}\boldsymbol{v}_q^{0,t}\boldsymbol{a}_w^{0,t}\Phi^{rt}(w,w,p,q)$$

$$+ \sum_{r=1}^{R}\sum_{t=1}^{T}\sum_{m=1}^{N_u-1}\sum_{p=0}^{N_F-1}\sum_{q=0}^{N_F-1} v_p^{0,1,T,TX} Z^{r,TX}[wN_F + p]\sqrt{P^{m,t}[wN_F + q]}\boldsymbol{v}_q^{m,t}\boldsymbol{a}_w^{m,t}(w,w,p,q)$$

$$+ \sum_{r=1}^{R}\sum_{t=1}^{T}\sum_{\substack{u=0 \\ u\neq w}}^{U-1}\sum_{m=0}^{N_u-1}\sum_{p=0}^{N_F-1}\sum_{q=0}^{N_F-1} v_p^{0,1,T,TX} Z^{r,TX}[wN_F + p]\sqrt{P^{m,t}[uN_F + q]}\boldsymbol{v}_q^{m,t}\boldsymbol{a}_u^{m,t}\Phi^{rt}(w,u,p,q)$$

$$+ \sum_{r=1}^{R}\sum_{p=0}^{N_F-1} v_p^{0,1,T,TX} Z^{r,TX}[wN_F + p].n^{r}[wN_F + p] \qquad = A + B + C + D$$

APPENDIX C

$$E[|A|^2] = E\left[\frac{1}{N_F}\sum_{r=1}^{R}\sum_{t=1}^{T} \boldsymbol{v}^{0,1,T,TX}\boldsymbol{Z}^{r,TX}[w]\boldsymbol{\Psi}^{rt}[w,w]\,\boldsymbol{P}^{0,t}[w]\,\boldsymbol{V}^{0,t}.a_w^{0,t}.a_w^{0,H,t}.\boldsymbol{V}^{0,H,t}.\boldsymbol{P}^{0,H,t}[w].\boldsymbol{\Psi}^{H,rt}[w,w]\boldsymbol{Z}^{H,r,TX}[w]\boldsymbol{v}^{0,1,T,H,TX}\right]$$

$$E[|B|^2] = E\left[\frac{1}{N_F}\sum_{r=1}^{R}\sum_{t=1}^{T} \boldsymbol{v}^{0,1,T,TX}.\,\boldsymbol{Z}^{r,TX}[w].\boldsymbol{\Psi}^{rt}[w,w].\boldsymbol{Q}^{t}[w].\,\boldsymbol{U}^{t}[w].\,\boldsymbol{a}_w^{t}.\boldsymbol{a}_w^{H,t}.\boldsymbol{U}^{H,t}[w].\boldsymbol{Q}^{H,t}[w].\boldsymbol{\Psi}^{H,rt}[w,w]\boldsymbol{Z}^{H,r,TX}[w]\boldsymbol{v}^{0,1,T,H,TX}\right]$$

$$E[|C|^2] = E\left[\frac{1}{N_F}\sum_{r=1}^{R}\sum_{t=1}^{T}\sum_{\substack{u=0\\u\neq w}}^{U-1} \boldsymbol{v}^{0,1,T,TX}.\,\boldsymbol{Z}^{r,TX}[w].\boldsymbol{\Psi}^{rt}[w,u].\boldsymbol{Q}^{t}[u].\,\boldsymbol{C}^{t}[u]\,.\,\boldsymbol{a}_u^{t}.\boldsymbol{a}_u^{H,t}.\boldsymbol{C}^{H,t}[u].\boldsymbol{Q}^{H,t}[u].\boldsymbol{\Psi}^{H,rt}[w,u]\boldsymbol{Z}^{H,r,TX}[w]\boldsymbol{v}^{0,1,T,H,TX}\right]$$

$$E[|D|^2] = E\left[\tfrac{1}{N_F}\textstyle\sum_{r=1}^{R} \boldsymbol{v}^{0,1,T,TX}.\,\boldsymbol{Z}^{r,TX}[w].\boldsymbol{n}^{r}[w]\,.\boldsymbol{n}^{H,r}[w].\boldsymbol{Z}^{H,r,TX}[w].\boldsymbol{v}^{0,1,T,H,TX}\right]$$

Equations above show that the SINR depends in a complex approach on the real spreading code. Then, they are difficult to apply practically. To eliminate this dependence, we will employ the asymptotic regime. Initially, this asymptotic behavior has been implemented by Tse and Hanly to the performance analysis of DS-CDMA systems with random spreading [45]. They realized that the dependence of the SINR on the spreading codes was fading in an asymptotic behavior (when N_F and$N_u \to \infty$ the ratio $\alpha = \frac{N_u}{N_F}$remains constant).

In order to evaluate the different terms of (44) independently of the spreading codes, we apply three properties from the RM and FP theories. With these properties, the equations yields for for a given CPN value:

$$E[|A|^2] = E\left[trace\left(\frac{1}{N_F}\sum_{r=1}^{R}\sum_{t=1}^{T}\boldsymbol{Z}^{r,TX}[w]\boldsymbol{\Psi}^{rt}[w,w]\,\boldsymbol{P}^{0,t}[w]\,\boldsymbol{V}^{0,t}.a_w^{0,t}.a_w^{0,H,t}.\boldsymbol{V}^{0,H,t}.\boldsymbol{P}^{0,H,t}[w].\boldsymbol{\Psi}^{H,rt}[w,w]\boldsymbol{Z}^{H,r,TX}[w]\right)\right]$$

$$= E\left[\frac{1}{N_F}\sum_{r=1}^{R}\sum_{t=1}^{T} trace\left(\boldsymbol{Z}^{r,TX}[w]\boldsymbol{\Psi}^{rt}[w,w]\,\boldsymbol{P}^{0,t}[w]\boldsymbol{V}^{0,t}.a_w^{0,t}.a_w^{0,H,t}.\boldsymbol{V}^{0,H,t}.\boldsymbol{P}^{0,H,t}[w].\boldsymbol{\Psi}^{H,rt}[w,w]\boldsymbol{Z}^{H,r,TX}[w]\right)\right]$$

$$= \frac{1}{N_F}\sum_{r=1}^{R}\sum_{t=1}^{T}\left[trace\left(\boldsymbol{Z}^{r,TX}[w]\boldsymbol{\Psi}^{rt}[w,w]\,\boldsymbol{P}^{0,t}[w]\,.\boldsymbol{P}^{0,H,t}[w].\boldsymbol{\Psi}^{H,rt}[w,w]\boldsymbol{Z}^{H,r,TX}[w]\right).trace\left\{E\left[\left(\boldsymbol{V}^{0,t}.a_w^{0,t}.a_w^{0,H,t}.\boldsymbol{V}^{0,H,t}\right)\right]\right\}\right]$$

$$= \frac{1}{N_F}\sum_{r=1}^{R}\sum_{t=1}^{T}\left[trace\left(\boldsymbol{Z}^{r,TX}[w]\boldsymbol{\Psi}^{rt}[w,w]\,\boldsymbol{P}^{0,t}[w]\,.\boldsymbol{P}^{0,H,t}[w].\boldsymbol{\Psi}^{H,rt}[w,w]\boldsymbol{Z}^{H,r,TX}[w]\right).trace\left(\boldsymbol{V}^{0,t}.\boldsymbol{V}^{0,H,t}\right)\right]$$

$$= \frac{1}{N_F}.trace\left(\boldsymbol{V}^{0,t}.\boldsymbol{V}^{0,H,t}\right).\sum_{r=1}^{R}\sum_{t=1}^{T} trace\left(\boldsymbol{Z}^{r,TX}[w]\boldsymbol{\Psi}^{rt}[w,w]\,\boldsymbol{P}^{0,t}[w]\,.\boldsymbol{P}^{0,H,t}[w].\boldsymbol{\Psi}^{H,rt}[w,w]\boldsymbol{Z}^{H,r,TX}[w]\right)$$

$$= \frac{1}{N_F}.trace\left(\sum_{r=1}^{R}\sum_{t=1}^{T}\boldsymbol{Z}^{r,TX}[w]\boldsymbol{\Psi}^{rt}[w,w]\,\boldsymbol{P}^{0,t}[w]\,.\boldsymbol{P}^{0,H,t}[w].\boldsymbol{\Psi}^{H,rt}[w,w]\boldsymbol{Z}^{H,r,TX}[w]\right).trace\left(\boldsymbol{V}^{0,t}.\boldsymbol{V}^{0,H,t}\right)$$

$$trace\left(\boldsymbol{V}^{0,t}.\boldsymbol{V}^{0,H,t}\right) = W$$

$$\boldsymbol{Z}\,[w] = diag(Z[wN_F], \dots, Z[wN_F + N_F - 1])$$

$$\boldsymbol{\Psi}[w,w] = \begin{pmatrix} \Phi(w,w,0,0) & \dots & \Phi(w,w,0,N_F-1) \\ \vdots & \ddots & \vdots \\ \Phi(w,w,N_F-1,0) & \dots & \Phi(w,w,N_F-1,N_F-1) \end{pmatrix}$$

$$\boldsymbol{P}^0[w] = diag\left(\sqrt{P_0^0}, \dots, \sqrt{P_{N_F-1}^0}\right)$$

$$\boldsymbol{O}[w] = \boldsymbol{Z}[w]\,\boldsymbol{\Psi}[w,w]$$

$$\boldsymbol{O}[w] = \begin{pmatrix} Z[wN_F]\Phi(w,w,0,0) & \dots & Z[wN_F]\Phi(w,w,0,N_F-1) \\ \vdots & \ddots & \vdots \\ Z[wN_F+N_F-1]\Phi(w,w,N_F-1,0) & \dots & Z[wN_F+N_F-1]\Phi(w,w,N_F-1,N_F-1) \end{pmatrix}$$

$$\boldsymbol{L}[w] = \boldsymbol{O}[w]\boldsymbol{P}^0[w]$$

$$\boldsymbol{L}[w] = \boldsymbol{O}[w]$$

$$\boldsymbol{F}[w] = \boldsymbol{L}[w]\boldsymbol{L}^H[w]$$

$$trace(\boldsymbol{F}[w]) = \sum_{r=1}^{R}\sum_{t=1}^{T}\sum_{k=0}^{N_F-1}\boldsymbol{F}_{kk}^{r,t}[w] = \sum_{r=1}^{R}\sum_{t=1}^{T}\sum_{k=0}^{N_F-1}\left|\boldsymbol{L}_{kk}^{r,t}[w]\right|^2$$

$$= \sum_{r=1}^{R}\sum_{t=1}^{T}\sum_{k=0}^{N_F-1}\left|\sum_{i=0}^{N_F-1}\boldsymbol{O}_{ki}^{r,t}[w]\boldsymbol{P}_{ik}^{0,t}[w]\right|^2$$

$$= \sum_{r=1}^{R}\sum_{t=1}^{T}\sum_{k=0}^{N_F-1}\left|\sum_{i=0}^{N_F-1}\left(\sum_{j=0}^{N_F-1}\boldsymbol{Z}_{kj}^{r,TX}[w]\boldsymbol{\Psi}_{ji}^{r,t}[w,w]\right)\boldsymbol{P}_{ik}^{0,t}[w]\right|^2$$

$$= \sum_{r=1}^{R}\sum_{t=1}^{T}\sum_{k=0}^{N_F-1}\left|\sum_{i=0}^{N_F-1}\boldsymbol{Z}_{kk}^{r,TX}[w]\boldsymbol{\Psi}_{ki}^{r,t}[w,w]\boldsymbol{P}_{ik}^{0,t}[w]\right|^2 = \sum_{r=1}^{R}\sum_{t=1}^{T}\sum_{k=0}^{N_F-1}\left|\boldsymbol{Z}_{kk}^{r,TX}[w]\boldsymbol{\Psi}_{kk}^{r,t}[w,w]\right|^2$$

$$= \sum_{r=1}^{R}\sum_{t=1}^{T}\sum_{p=0}^{N_F-1}|Z^{r,TX}[wN_F+p]\Phi^{r,t}(w,w,p,p)|^2$$

$$= \sum_{r=1}^{R}\sum_{t=1}^{T}\sum_{p=0}^{N_F-1}\left|\frac{1}{\Phi^{r,TX}(w,w,p,p)}.\Phi^{r,t}(w,w,p,p)\right|^2$$

$$= T.R.N_F$$

$$E[|A|^2] = \frac{1}{N_F}.trace(\boldsymbol{F}[w]) \times trace\left(\boldsymbol{V}^{0,t}.\boldsymbol{V}^{0,H,t}\right)$$

$$\boxed{E[|A|^2] = T.R.W}$$

$$E[|B|^2]$$

$$= \frac{1}{N_F}.trace\left(\sum_{r=1}^{R}\sum_{t=1}^{T} \boldsymbol{Z}^{r,TX}[w].\boldsymbol{\Psi}^{rt}[w,w].\boldsymbol{Q}^{t}[w].\ \boldsymbol{U}^{t}[w].\ \boldsymbol{a}_w^t.\boldsymbol{a}_w^{H,t}.\boldsymbol{U}^{H,t}[w].\boldsymbol{Q}^{H,t}[w].\boldsymbol{\Psi}^{H,rt}[w,w]\boldsymbol{Z}^{H,r,TX}[w] \right)$$

$$= \frac{1}{N_F}.\sum_{r=1}^{R}\sum_{t=1}^{T} trace\left(\boldsymbol{Z}^{r,TX}[w].\boldsymbol{\Psi}^{rt}[w,w].\boldsymbol{Q}^{t}[w].\ \boldsymbol{U}^{t}[w].\ \boldsymbol{a}_w^t.\boldsymbol{a}_w^{H,t}.\boldsymbol{U}^{H,t}[w].\boldsymbol{Q}^{H,t}[w].\boldsymbol{\Psi}^{H,rt}[w,w]\boldsymbol{Z}^{H,r,TX}[w] \right)$$

$$= \frac{1}{N_F}.\sum_{r=1}^{R}\sum_{t=1}^{T} \left[trace\left(\boldsymbol{Z}^{r,TX}[w].\boldsymbol{\Psi}^{rt}[w,w].\boldsymbol{Q}^{t}[w].\boldsymbol{Q}^{H,t}[w].\boldsymbol{\Psi}^{H,rt}[w,w]\boldsymbol{Z}^{H,r,TX}[w] \right).trace\left(\boldsymbol{U}^{t}[w].\ \boldsymbol{a}_w^t.\boldsymbol{a}_w^{H,t}.\boldsymbol{U}^{H,t}[w] \right) \right]$$

$$= \frac{1}{N_F}.\sum_{r=1}^{R}\sum_{t=1}^{T} \left[trace\left(\boldsymbol{Z}^{r,TX}[w].\boldsymbol{\Psi}^{rt}[w,w].\boldsymbol{Q}^{t}[w].\boldsymbol{Q}^{H,t}[w].\boldsymbol{\Psi}^{H,rt}[w,w]\boldsymbol{Z}^{H,r,TX}[w] \right).trace\left(\boldsymbol{U}^{t}[w].\boldsymbol{U}^{H,t}[w] \right) \right]$$

$$= \frac{1}{N_F}.\sum_{r=1}^{R}\sum_{t=1}^{T} \left[trace\left(\boldsymbol{Z}^{r,TX}[w].\boldsymbol{\Psi}^{rt}[w,w].\boldsymbol{Q}^{t}[w].\boldsymbol{Q}^{H,t}[w].\boldsymbol{\Psi}^{H,rt}[w,w]\boldsymbol{Z}^{H,r,TX}[w] \right).trace\left(\alpha.W.I - \boldsymbol{V}^{0,t}.\boldsymbol{V}^{0,H,t} \right) \right]$$

$$= \frac{1}{N_F}.W(N_u-1).\sum_{r=1}^{R}\sum_{t=1}^{T} trace\left(\boldsymbol{Z}^{r,TX}[w].\boldsymbol{\Psi}^{rt}[w,w].\boldsymbol{Q}^{t}[w].\boldsymbol{Q}^{H,t}[w].\boldsymbol{\Psi}^{H,rt}[w,w]\boldsymbol{Z}^{H,r,TX}[w] \right)$$

$$= \frac{1}{N_F}.W(N_u-1).trace\left(\sum_{r=1}^{R}\sum_{t=1}^{T} \boldsymbol{Z}^{r,TX}[w].\boldsymbol{\Psi}^{rt}[w,w].\boldsymbol{Q}^{t}[w].\boldsymbol{Q}^{H,t}[w].\boldsymbol{\Psi}^{H,rt}[w,w]\boldsymbol{Z}^{H,r,TX}[w] \right)$$

$$\boldsymbol{Q}\ [w] = \begin{pmatrix} \sqrt{P_0^1} & \sqrt{P_0^2} & \cdots & \sqrt{P_0^{N_u-1}} \\ \vdots & \vdots & \cdots & \vdots \\ \sqrt{P_{N_F-1}^1} & \sqrt{P_{N_F-1}^2} & \cdots & \sqrt{P_{N_F-1}^{N_u-1}} \end{pmatrix}$$

$$\boldsymbol{D}[w] = \boldsymbol{O}[w]\boldsymbol{Q}\ [w]$$

$$\boldsymbol{D}[w] = \begin{pmatrix} \sum_{q=0}^{N_F-1} Z[wN_F]\Phi(w,w,0,q) & \cdots & \sum_{q=0}^{N_F-1} Z[wN_F]\Phi(w,w,0,q) \\ \vdots & \ddots & \vdots \\ \sum_{q=0}^{N_F-1} Z[wN_F+N_F-1]\Phi(w,w,N_F-1,q) & \cdots & \sum_{q=0}^{N_F-1} Z[wN_F+N_F-1]\Phi(w,w,N_F-1,q) \end{pmatrix}$$

$$\boldsymbol{D}[w]\ is\ (N_F) \times (N_u-1)$$

$$\boldsymbol{E}[w] = \boldsymbol{D}[w]\boldsymbol{D}^H[w]$$

$$trace(\boldsymbol{E}[w])$$
$$= \sum_{r=1}^{R}\sum_{t=1}^{T}\sum_{k=0}^{N_F-1} \boldsymbol{E}_{kk}^{r,t}[w]$$
$$= \sum_{r=1}^{R}\sum_{t=1}^{T}\sum_{k=0}^{N_F-1} N_F\left|\boldsymbol{D}_{kk}^{r,t}[w]\right|^2$$
$$= \sum_{r=1}^{R}\sum_{t=1}^{T}\sum_{k=0}^{N_F-1} N_F\left|\gamma \sum_{i=0}^{N_F-1} \boldsymbol{Z}_{kk}^{r,TX}[w]\boldsymbol{\Psi}_{ki}^{r,t}[w,w]\right|^2$$
$$= N_F\sum_{r=1}^{R}\sum_{t=1}^{T}\sum_{p=0}^{N_F-1}\left|\gamma \sum_{q=0}^{N_F-1} Z^{r,TX}[wN_F\, p]\Phi^{r,t}(w,w,p,q)\right|^2$$
$$= N_F\sum_{r=1}^{R}\sum_{t=1}^{T}\sum_{p=0}^{N_F-1}\left|\gamma \sum_{q=0}^{N_F-1} \frac{\Phi^{r,t}(w,w,p,q)}{\Phi^{r,TX}(w,w,p,p)}\right|^2$$
$$= N_F\sum_{r=1}^{R}\sum_{t=1}^{T}\sum_{p=0}^{N_F-1}\left|\gamma \sum_{q=0}^{N_F-1} \frac{h^{r,t}[wN_F+q]\ \sum_{k=0}^{N-1} e^{-\frac{j2\pi(p-q)k}{N}} e^{j\theta[k]}}{h^{r,TX}[wN_F+p]\ \sum_{v=0}^{N-1} e^{j\theta[v]}}\right|^2$$

$$0 \le \gamma \le 1, \begin{cases} 0, the\ performance\ of\ the\ MPA\ receiver\ is\ 100\% \\ 1, the\ performance\ of\ the\ MPA\ receiver\ is\ 0\% \end{cases}$$

In Rayleigh:

$$E[|B|^2] = \frac{1}{N_F} trace(\boldsymbol{E}[w])$$
$$= \frac{1}{N_F}.W.(N_u-1).N_F\sum_{r=1}^{R}\sum_{t=1}^{T}\sum_{p=0}^{N_F-1}\left|\gamma \sum_{q=0}^{N_F-1} \frac{h^{r,t}[wN_F+q]\ \sum_{k=0}^{N-1} e^{-\frac{j2\pi(p-q)k}{N}} e^{j\theta[k]}}{h^{r,TX}[wN_F+p]\ \sum_{v=0}^{N-1} e^{j\theta[v]}}\right|^2$$

$$E[|B|^2] = W.(N_u-1).\sum_{r=1}^{R}\sum_{t=1}^{T}\sum_{p=0}^{N_F-1}\left|\gamma \sum_{q=0}^{N_F-1} \frac{h^{r,t}[wN_F+q]\ \sum_{k=0}^{N-1} e^{-\frac{j2\pi(p-q)k}{N}} e^{j\theta[k]}}{h^{r,TX}[wN_F+p]\ \sum_{v=0}^{N-1} e^{j\theta[v]}}\right|^2$$

In AWGN:

$$h[wN_F+q] = h[wN_F+p] = 1$$

$$E[|B|^2] = T.R.W.(N_u-1).\sum_{p=0}^{N_F-1}\left|\gamma \sum_{q=0}^{N_F-1} \frac{\sum_{k=0}^{N-1} e^{-\frac{j2\pi(p-q)k}{N}} e^{j\theta[k]}}{\sum_{v=0}^{N-1} e^{j\theta[v]}}\right|^2$$

$$E[|C|^2] = \frac{1}{N_F} trace\left(\sum_{r=1}^{R} \sum_{t=1}^{T} \sum_{\substack{u=0 \\ u \neq w}}^{U-1} \boldsymbol{Z}^{r,TX}[w].\boldsymbol{\Psi}^{rt}[w,u].\boldsymbol{Q}^{t}[u].\boldsymbol{C}^{t}[u].\boldsymbol{a}_u^{t}.\boldsymbol{a}_u^{H,t}.\boldsymbol{C}^{H,t}[u].\boldsymbol{Q}^{H,t}[u].\boldsymbol{\Psi}^{H,rt}[w,u]\boldsymbol{Z}^{H,r,TX}[w] \right)$$

$$= \frac{1}{N_F} \sum_{r=1}^{R} \sum_{t=1}^{T} \sum_{\substack{u=0 \\ u \neq w}}^{U-1} trace\left(\boldsymbol{Z}^{r,TX}[w].\boldsymbol{\Psi}^{rt}[w,u].\boldsymbol{Q}^{t}[u].\boldsymbol{C}^{t}[u].\boldsymbol{a}_u^{t}.\boldsymbol{a}_u^{H,t}.\boldsymbol{C}^{H,t}[u].\boldsymbol{Q}^{H,t}[u].\boldsymbol{\Psi}^{H,rt}[w,u]\boldsymbol{Z}^{H,r,TX}[w]\right)$$

$$= \frac{1}{N_F} \sum_{r=1}^{R} \sum_{t=1}^{T} \sum_{\substack{u=0 \\ u \neq w}}^{U-1} trace(\boldsymbol{Z}^{r,TX}[w].\boldsymbol{\Psi}^{rt}[w,u].\boldsymbol{Q}^{t}[u].\boldsymbol{Q}^{H,t}[u].\boldsymbol{\Psi}^{H,rt}[w,u]\boldsymbol{Z}^{H,r,TX}[w]).trace\left(E\left(\boldsymbol{C}^{t}[u].\boldsymbol{a}_u^{t}.\boldsymbol{a}_u^{H,t}.\boldsymbol{C}^{H,t}[u]\right)\right)$$

$$= \frac{1}{N_F} \sum_{r=1}^{R} \sum_{t=1}^{T} \sum_{\substack{u=0 \\ u \neq w}}^{U-1} trace(\boldsymbol{Z}^{r,TX}[w].\boldsymbol{\Psi}^{rt}[w,u].\boldsymbol{Q}^{t}[u].\boldsymbol{Q}^{H,t}[u].\boldsymbol{\Psi}^{H,rt}[w,u]\boldsymbol{Z}^{H,r,TX}[w]).W.N_u$$

$$= \frac{1}{N_F}.W.N_u.trace\left(\sum_{r=1}^{R} \sum_{t=1}^{T} \sum_{\substack{u=0 \\ u \neq w}}^{U-1} \boldsymbol{Z}^{r,TX}[w].\boldsymbol{\Psi}^{rt}[w,u].\boldsymbol{Q}^{t}[u].\boldsymbol{Q}^{H,t}[u].\boldsymbol{\Psi}^{H,rt}[w,u]\boldsymbol{Z}^{H,r,TX}[w] \right)$$

$$\boldsymbol{G}[u] = \sum_{\substack{u=0 \\ u \neq w}}^{U-1} \boldsymbol{E}[u]$$

$$trace(\boldsymbol{G}[u]) = \sum_{r=1}^{R} \sum_{t=1}^{T} \sum_{k=0}^{N_F-1} \sum_{\substack{u=0 \\ u \neq w}}^{U-1} \boldsymbol{E}_{kk}^{r,t}[u] = \sum_{r=1}^{R} \sum_{t=1}^{T} \sum_{k=0}^{N_F-1} \sum_{\substack{u=0 \\ u \neq w}}^{U-1} N_F \left| \sum_{\boldsymbol{i=0}}^{N_F-1} \boldsymbol{Z}_{kk}^{r,TX}[w] \boldsymbol{\Psi}_{ki}^{r,t}[w,u] \right|^2$$

$$= \sum_{r=1}^{R} \sum_{t=1}^{T} \sum_{p=0}^{N_F-1} \sum_{\substack{u=0 \\ u \neq w}}^{U-1} N_F \left| \sum_{\boldsymbol{q=0}}^{N_F-1} Z^{r,TX}[wN_F + p] \Phi^{r,t}(w,u,p,q) \right|^2$$

$$= \sum_{r=1}^{R} \sum_{t=1}^{T} \sum_{p=0}^{N_F-1} \sum_{\substack{u=0 \\ u \neq w}}^{U-1} N_F \left| \sum_{\boldsymbol{q=0}}^{N_F-1} \frac{\Phi^{r,t}(w,u,p,q)}{\Phi^{r,TX}(w,w,p,p)} \right|^2$$

$$= N_F \sum_{r=1}^{R} \sum_{t=1}^{T} \sum_{p=0}^{N_F-1} \sum_{\substack{u=0 \\ u \neq w}}^{U-1} \left| \sum_{\boldsymbol{q=0}}^{N_F-1} \frac{h^{r,t}[uN_F + q] \sum_{k=0}^{N-1} e^{-\frac{j2\pi k((w-u)N_F + (p-q))}{N}} e^{j\theta[k]}}{h^{r,TX}[wN_F + p] \sum_{v=0}^{N-1} e^{j\theta[v]}} \right|^2$$

In Rayleigh:

$$E[|C|^2] = \frac{1}{N_F} trace(\boldsymbol{G}[u]).W.N_u$$

$$= W.N_u \sum_{r=1}^{R} \sum_{t=1}^{T} \sum_{p=0}^{N_F-1} \sum_{\substack{u=0 \\ u \neq w}}^{U-1} \left| \sum_{\boldsymbol{q=0}}^{N_F-1} \frac{h^{r,t}[uN_F + q] \sum_{k=0}^{N-1} e^{-\frac{j2\pi k((w-u)N_F + (p-q))}{N}} e^{j\theta[k]}}{h^{r,TX}[wN_F + p] \sum_{v=0}^{N-1} e^{j\theta[v]}} \right|^2$$

$$E[|C|^2] = W.N_u \sum_{r=1}^{R} \sum_{t=1}^{T} \sum_{p=0}^{N_F-1} \sum_{\substack{u=0 \\ u \neq w}}^{U-1} \left| \sum_{\boldsymbol{q=0}}^{N_F-1} \frac{h^{r,t}[uN_F + q] \sum_{k=0}^{N-1} e^{-\frac{j2\pi k((w-u)N_F + (p-q))}{N}} e^{j\theta[k]}}{h^{r,TX}[wN_F + p] \sum_{v=0}^{N-1} e^{j\theta[v]}} \right|^2$$

In AWGN:

$$h[uN_F + q] = h[wN_F + p] = 1$$

$$E[|C|^2] = T.R.W.N_u \sum_{p=0}^{N_F-1} \sum_{\substack{u=0 \\ u\neq w}}^{U-1} \left| \sum_{\boldsymbol{q=0}}^{N_F-1} \frac{\sum_{k=0}^{N-1} e^{-\frac{j2\pi k\left((w-u)N_F+(p-q)\right)}{N}} e^{j\theta[k]}}{\sum_{v=0}^{N-1} e^{j\theta[v]}} \right|^{\mathbf{2}}$$

$$E[|D|^2] = trace\left(\sum_{r=1}^{R} \boldsymbol{Z}^{r,TX}[w].\boldsymbol{n}^{r}[w].\boldsymbol{n}^{H,r}[w].\boldsymbol{Z}^{H,r,TX}[w] \right)$$

$$= \sigma^2 trace\left(\sum_{r=1}^{R} \boldsymbol{Z}^{r,TX}[w].\boldsymbol{Z}^{H,r,TX}[w] \right)$$

$$E[|D|^2] = \frac{\sigma^2}{N_F} trace\left(\sum_{r=1}^{R} \boldsymbol{Z}^{r,TX}[w].\boldsymbol{Z}^{H,r,TX}[w] \right)$$

$$\boldsymbol{S}[w] = \boldsymbol{Z}[w]\boldsymbol{n}[w]$$

$$\boldsymbol{T}[w] = \boldsymbol{S}[w]\boldsymbol{S}^{H}[w]$$

$$trace(\boldsymbol{T}[w]) = \sum_{r=1}^{R} \sum_{i=0}^{N_F-1} \boldsymbol{T}_{ii}^{r,TX}[w] = \sum_{r=1}^{R} \sum_{i=0}^{N_F-1} \left|\boldsymbol{S}_{ii}^{r,TX}[w]\right|^{\mathbf{2}} = \sum_{r=1}^{R} \sum_{i=0}^{N_F-1} \left|\boldsymbol{Z}_{ii}^{r,TX}[w]\boldsymbol{n}_{i}^{r}[w]\right|^{\mathbf{2}}$$

$$= \sum_{r=1}^{R} \sum_{p=0}^{N_F-1} |\boldsymbol{Z}^{r,TX}[wN_F+p]\boldsymbol{n}^{r}[wN_F+p]|^{\mathbf{2}} = \sum_{r=1}^{R} \sum_{p=0}^{N_F-1} |\boldsymbol{Z}^{r,TX}[wN_F+p]|^{\mathbf{2}}$$

$$= \sigma^2 \sum_{r=1}^{R} \sum_{p=0}^{N_F-1} \left| \frac{1}{\Phi^{r,TX}(w,w,p,p)} \right|^{\mathbf{2}}$$

$$= \sigma^2 \sum_{r=1}^{R} \sum_{p=0}^{N_F-1} \left| \frac{N}{h^{r,TX}[wN_F+p] \sum_{k=0}^{N-1} e^{j\theta[k]}} \right|^{\mathbf{2}} = \sigma^2 \sum_{r=1}^{R} \sum_{p=0}^{N_F-1} \left| \frac{1}{h^{r,TX}[wN_F+p].CPE} \right|^{\mathbf{2}}$$

In Rayleigh:

$$\boxed{E[|D|^2] = \frac{\sigma^2}{N_F} \sum_{r=1}^{R} \sum_{p=0}^{N_F-1} \left| \frac{1}{h^{r,TX}[wN_F+p].CPE} \right|^{\mathbf{2}}}$$

In AWGN:

$h[wN_F+p] = 1$

$$\boxed{E[|D|^2] = \frac{\sigma^2.R}{|CPE|^2}}$$

REFERENCES

[1] Lee, B. M., Choi, J., Bang, J., & Kang, B. C. (2013, May). An energy efficient antenna selection for large scale green MIMO systems. In *2013 IEEE International Symposium on Circuits and Systems (ISCAS2013)* (pp. 950-953). IEEE.

[2] Zhou, Z., Ge, N., & Lin, X. (2014). Reduced-complexity antenna selection schemes in spatial modulation. *IEEE Communications Letters*, *18*(1), 14-17.

[3] Larsson, E. G., Edfors, O., Tufvesson, F., & Marzetta, T. L. (2014). Massive MIMO for next generation wireless systems. *IEEE Communications Magazine*, *52*(2), 186-195.

[4] Rusek, F., Persson, D., Lau, B. K., Larsson, E. G., Marzetta, T. L., Edfors, O., & Tufvesson, F. (2013). Scaling up MIMO: Opportunities and challenges with very large arrays. *IEEE Signal Processing Magazine*, *30*(1), 40-60.

[5] Gesbert, D., Kountouris, M., Heath Jr, R. W., Chae, C. B., & Salzer, T. (2007). Shifting the MIMO paradigm. *IEEE signal processing magazine*, *24*(5), 36-46.

[6] You, C., Hwang, I., Kim, Y., & Tarokh, V. (2009). Dual antenna selection algorithms and feedback strategies with reduced complexity for multiple-input multiple-output systems. *IET microwaves, antennas & propagation*, *3*(6), 906-916.

[7] Torabi, M. (2008). Antenna selection for MIMO-OFDM systems. *Signal Processing*, *88*(10), 2431-2441.

[8] Zhang, J., & De la Roche, G. (2010). *Femtocells: technologies and deployment* (pp. 1-13). New York: Wiley.

[9] Network, T. S. G. R. A. (2009). Tr 36.814-further advancements for e-utra: Physical layer aspects (release 9). *3rd Generation Partnership Project Tech. Rep., Tech. Rep*.

[10] Prasad, R., & Ruggieri, M. (2003). *Technology trends in wireless communications*. Artech House.

[11] Nikopour, H., & Baligh, H. (2013, September). Sparse code multiple access. In *2013 IEEE 24th Annual International Symposium on Personal, Indoor, and Mobile Radio Communications (PIMRC)* (pp. 332-336). IEEE.

[12] Taherzadeh, M., Nikopour, H., Bayesteh, A., & Baligh, H. (2014, September). SCMA codebook design. In *2014 IEEE 80th Vehicular Technology Conference (VTC2014-Fall)* (pp. 1-5). IEEE.

[13] Raut, P. W., & Badjate, S. (2013). MIMO-future wireless communication. *International Journal of Innovative Technology and Exploring Engineering (IJITEE)*, *2*(5), 102-106.

[14] Massive MIMO Info Point. *Massivemimo.eu*. N.p., 2015. Accessed[12 July 2015].

[15] Ngo, H. Q., & Larsson, E. G. (2012, March). EVD-based channel estimation in multicell multiuser MIMO systems with very large antenna arrays. In *2012 IEEE International Conference on Acoustics, Speech and Signal Processing (ICASSP)* (pp. 3249-3252). IEEE.

[16] Kudo, R., Armour, S. M., McGeehan, J. P., & Mizoguchi, M. (2012, August). CSI estimation method based on random beamforming for massive number of transmit antenna systems. In *2012 International Symposium on Wireless Communication Systems (ISWCS)* (pp. 716-720). IEEE.

[17] Lu, Y., & Zhang, W. (2013, April). Water-filling capacity analysis in large MIMO systems. In *Computing, Communications and IT Applications Conference (ComComAp), 2013* (pp. 186-190). IEEE.

[18] Gkizeli, M., & Karystinos, G. N. (2014). Maximum-SNR antenna selection among a large number of transmit antennas. *IEEE Journal of Selected Topics in Signal Processing*, *8*(5), 891-901.

[19] Mueller, A., Kammoun, A., Björnson, E., & Debbah, M. (2016). Linear precoding based on polynomial expansion: Reducing complexity in massive MIMO. *EURASIP Journal on Wireless Communications and Networking*, *2016*(1), 1.

[20] Hoydis, J. (2013). Massive MIMO and HetNets: Benefits and challenges. *Newcom# Summer School on Interference Management for Tomorrow's Wireless Networks*.

[21] Marzetta, T. L. (2010). Noncooperative cellular wireless with unlimited numbers of base station antennas. *IEEE Transactions on Wireless Communications*, *9*(11), 3590-3600.

[22] Müller, R. R., Cottatellucci, L., & Vehkaperä, M. (2014). Blind pilot decontamination. *IEEE Journal of Selected Topics in Signal Processing*, *8*(5), 773-786.

[23] Ngo, H. Q., & Larsson, E. G. (2012). EVD-based Channel Estimations for Multicell Multiuser MIMO with Very Large Antenna Arrays PDF.

[24] Ashikhmin, A., & Marzetta, T. (2012, July). Pilot contamination precoding in multi-cell large scale antenna systems. In *Information Theory Proceedings (ISIT), 2012 IEEE International Symposium on* (pp. 1137-1141). IEEE.

[25] Fernandes, F., Ashikhmin, A., & Marzetta, T. L. (2013). Inter-cell interference in noncooperative TDD large scale antenna systems. *IEEE Journal on Selected Areas in Communications*, *31*(2), 192-201.

[26] Lee, J., Han, J. K., & Zhang, J. C. (2009). MIMO technologies in 3GPP LTE and LTE-advanced. *EURASIP Journal on Wireless Communications and Networking*, *2009*(1), 1-10.

[27] Duplicy, J., Badic, B., Balraj, R., Ghaffar, R., Horváth, P., Kaltenberger, F., ... & Vivier, G. (2011). Mu-mimo in lte systems. *EURASIP Journal on Wireless Communications and Networking*, *2011*(1), 1.

[28] Love, D. J., Heath, R. W., Lau, V. K., Gesbert, D., Rao, B. D., & Andrews, M. (2008). An overview of limited feedback in wireless communication systems. *IEEE Journal on Selected Areas in Communications*, *26*(8), 1341-1365.

[29] Hoshyar, R., Razavi, R., & Al-Imari, M. (2010, May). LDS-OFDM an efficient multiple access technique. In *Vehicular Technology Conference (VTC 2010-Spring), 2010 IEEE 71st* (pp. 1-5). IEEE.

[30] Forney, G. D., & Wei, L. F. (1989). Multidimensional constellations. I. Introduction, figures of merit, and generalized cross constellations. *IEEE journal on selected areas in communications*, *7*(6), 877-892.

[31] Dahlman, E., Parkvall, S., & Skold, J. (2013). *4G: LTE/LTE-advanced for mobile broadband*. Academic press.

[32] Nikopour, H., Yi, E., Bayesteh, A., Au, K., Hawryluck, M., Baligh, H., & Ma, J. (2014, December). SCMA for downlink multiple access of 5G wireless networks. In *2014 IEEE Global Communications Conference* (pp. 3940-3945). IEEE.

[33] Lu, L., Chen, Y., Guo, W., Yang, H., Wu, Y., & Xing, S. (2015). Prototype for 5G new air interface technology SCMA and performance evaluation. *China Communications*, *12*(Supplement), 38-48.

[34] Pollet, T., Van Bladel, M., & Moeneclaey, M. (1995). BER sensitivity of OFDM systems to carrier frequency offset and Wiener phase noise. *IEEE transactions on communications*, *43*(2/3/4), 191-193.

[35] Steendam, H., & Moeneclaey, M. (2000). Comparison of the sensitivities of MC-CDMA and MC-DS-CDMA to carrier frequency offset. In *Communications and Vehicular Technology, 2000. SCVT-200. Symposium on* (pp. 166-173). IEEE.

[36] Nasser, Y., Des Noes, M., Ros, L., & Jourdain, G. (2006, June). Sensitivity of OFDM-CDMA systems to carrier frequency offset. In *2006 IEEE International Conference on Communications* (Vol. 10, pp. 4577-4582). IEEE.

[37] Stott, J. (1998). The effects of phase noise in COFDM. *EBU technical Review*, 12-25.

[38] Armada, A. G. (2001). Understanding the effects of phase noise in orthogonal frequency division multiplexing (OFDM). *IEEE Transactions on Broadcasting*, *47*(2), 153-159.

[39] Steendam, H., & Moeneclaey, M. (1999). The effect of carrier phase jitter on MC-CDMA performance. *IEEE Transactions on Communications*, *47*(2), 195-198.

[40] Nasser, Y., Des Noes, M., Ros, L., & Jourdain, G. (2010). On the system level prediction of joint time frequency spreading systems with carrier phase noise. *IEEE Transactions on Communications*, *58*(3), 839-850.

[41] Nasser, Y., Des Noes, M., Ros, L., & Jourdain, G. (2006, July). Sensitivity of Multi Carrier 2 Dimensional Spreading systems to carrier phase noise. In *2006 IEEE 7th Workshop on Signal Processing Advances in Wireless Communications* (pp. 1-5). IEEE.

[42] Nasser, Y., Des Noes, M., Ros, L., & ve Jourdain, G. (2005, September). SINR estimation of OFDM-CDMA systems with constant timing offset: a large system analysis. In *2005 IEEE 16th International Symposium on Personal, Indoor and Mobile Radio Communications* (Vol. 1, pp. 432-436). IEEE.

[43] Nasser, Y., Des Noes, M., Ros, L., & Jourdain, G. (2005). The effect of clock frequency offset on OFDM-CDMA systems. In *Symposium on Communications and Vehicular Technology (SCVT'05)*.

[44] Mehrotra, A. (1999). *Simulation and modelling techniques for noise in radio frequency integrated circuits* (Doctoral dissertation, UNIVERSITY of CALIFORNIA at BERKELEY).

[45] Tse, D. N. C., & Hanly, S. V. (1999). Linear multiuser receivers: Effective interference, effective bandwidth and user capacity. *IEEE Transactions on Information Theory*, *45*(2), 641-657.

[46] Zhang, S., Xiao, B., Xiao, K., Chen, Z., & Xia, B. (2015, October). Design and analysis of irregular sparse code multiple access. In *Wireless Communications & Signal Processing (WCSP), 2015 International Conference on* (pp. 1-5). IEEE.

[47] Van De Beek, J., & Popovic, B. M. (2009, November). Multiple access with low-density signatures. In *Global Telecommunications Conference, 2009. GLOBECOM 2009. IEEE* (pp. 1-6). IEEE.